Bright and Effectual Perovskite Light Emitting Electrochemical Cells Leveraging Ionic Additives

Masoud Alahbakhshi[1], Aditya Mishra[2], Ross Haroldson[3], Arthur Ishteev[5,6], Jiyoung Moon[2], Qing Gu[1], Jason D. Slinker[2,3] and Anvar A. Zakhidov[3,4,5,6]**

[1]Department of Electrical and Computer Engineering, The University of Texas at Dallas, 800 West Campbell Road, Richardson, Texas 75080-3021, United States.

[2]Department of Materials Science and Engineering, The University of Texas at Dallas, 800 West Campbell Road, Richardson, Texas 75080-3021, United States.

[3]Department of Physics, The University of Texas at Dallas, 800 West Campbell Road, Richardson, Texas 75080-3021, United States.

[4]NanoTech Institute, The University of Texas at Dallas, 800 West Campbell Road, Richardson, Texas 75080-3021, United States.

[5]Department of Nanophotonics and Metamaterials, ITMO University, St. Petersburg, Moscow, Russia.

[6]Laboratory of Advanced Solar Energy, NUST MISiS, Moscow, 119049, Russia

AUTHOR INFORMATION

Corresponding Author

*slinker@utdallas.edu, *zakhidov@utdallas.edu

ABSTRACT: Perovskite light emitting diodes (PeLEDs) have drawn considerable attention for their favorable optoelectronic properties. Perovskite light emitting electrochemical cells (PeLECs) – devices that utilize mobile ions – have recently been reported but have yet to reach the performance of the best PeLEDs. We leveraged a poly(ethylene oxide) electrolyte and a lithium salt in $CsPbBr_3$ thin films to produce PeLECs of improved brightness and efficiency. In particular, we found that a single layer PeLEC from $CsPbBr_3$:PEO:$LiPF_6$ with 0.5% wt. $LiPF_6$ produced bright (~15000 cd/m^2) electroluminescence of improved efficiency (3.0 Lm/W). To understand this improved performance among PeLECs, we characterized these perovskite thin films with photoluminescence (PL) spectroscopy, scanning electron microscopy (SEM), atomic force microscopy (AFM), X-ray photoelectron spectroscopy (XPS), and X-ray diffraction (XRD). These studies revealed that this optimal $LiPF_6$ concentration improves electrical double layer formation, reduces the occurrence of voids, charge traps, and pinholes, and increases grain size and packing density.

TOC GRAPHICS

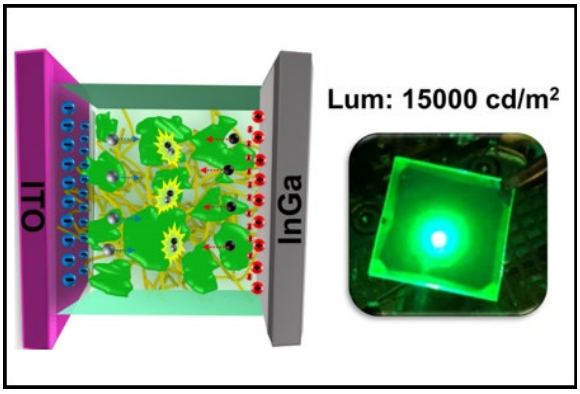

Perovskite light-emitting diodes (PeLEDs) based on inorgano−organometallic halide perovskites, such as $CH_3NH_3PbX_3$ and $CsPbX_3$ (X = Cl, Br, or I), have attracted much attention due to their low-temperature solution processability, high color purity with narrow spectral width (FWHM of 20 nm), band gap tunability and large charge carrier mobility.[1-4] To date, devices based on these perovskites have achieved high luminance in excess of 10000 cd/m^2 with high efficiencies (EQE ~10%), comparable to organic LEDs and quantum dot (QD) LEDs.[1-10]

Interestingly, effects such as hysteresis and high capacitance in perovskite semiconductor devices suggest that ion motion can largely influence device operation. In this vein, researchers have recently been investigating perovskite materials in light-emitting electrochemical cell (LEC) architectures instead of traditional LEDs.[11-15] These LEC devices (PeLEC) leverage ion redistribution to achieve balanced and high carrier injection, resulting in high electroluminescence efficiency. Due to this mechanism, LEC devices can be prepared from a simple architecture consisting of a single semiconducting composite layer sandwiched between two electrodes. In addition, they can operate at low voltages below the bandgap, yielding highly efficient devices. Recently, perovskite LECs (PeLECs) have been reported and show promise as electroluminescent devices.[11-15] However, these PeLECs are generally limited to luminance maxima of 1000 cd/m^2 or lower, below what has been typically observed in PeLEDs. This disparity suggests that further understanding and refinement of PeLEC materials and devices could produce significant improvements of brightness, efficiency, and other performance metrics. To this end, we fabricated a bright (~15000 cd/m^2) single layer LEC of improved efficiency (3.0 Lm/W) based on a cesium lead halide perovskite, $CsPbBr_3$. To achieve high performance, a polyelectrolyte and additive mobile ions were carefully selected to achieve optimal ionic redistribution and doping effects. To understand the nature of this performance and its correlation with materials properties, we

characterize these perovskite thin films and devices with photoluminescence spectroscopy, scanning electron microscopy (SEM), atomic force microscopy (AFM), X-ray photoelectron spectroscopy (XPS), and X-ray diffraction (XRD).

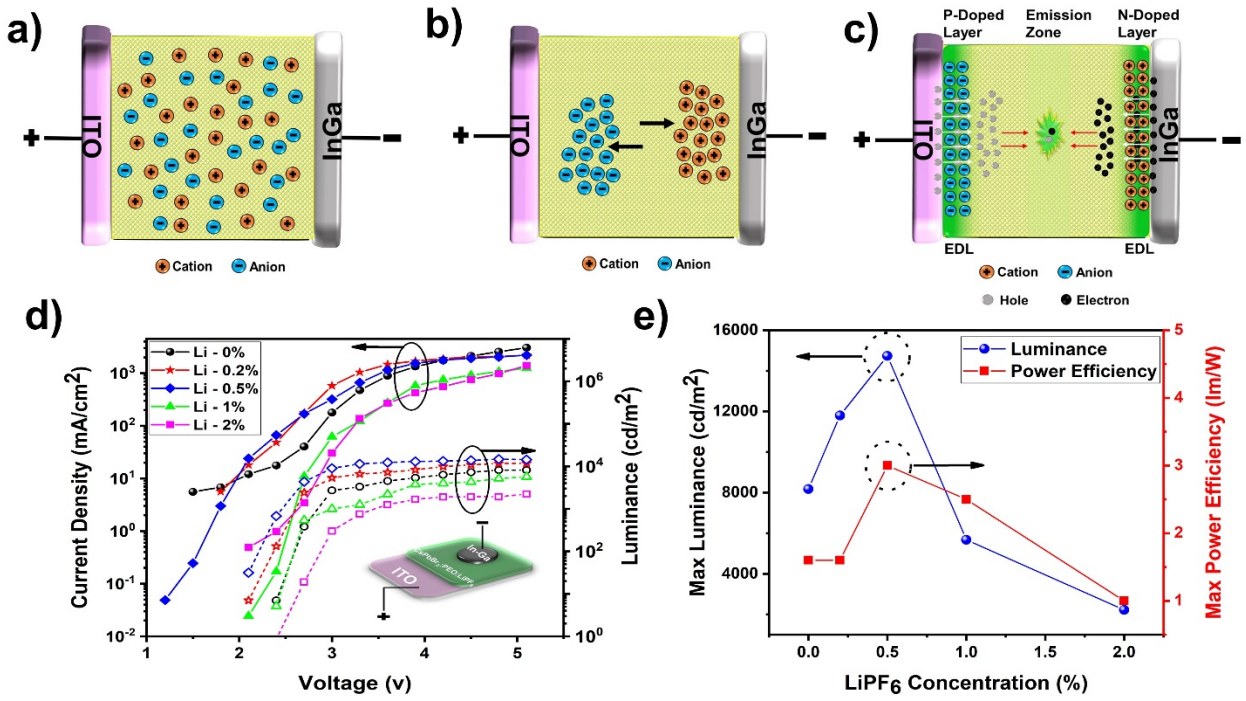

Figure 1. Illustration of PeLEC device operation and device characteristics. a) Initial LEC state showing ions uniformly distributed throughout the active layer. b) Intermediate LEC state showing cations drifting toward the cathode and anions toward the anode. c) Steady-state LEC operation with ions accumulated at the electrodes and light emission upon current injection. d) Current density and luminance versus voltage for In-Ga/$CsPbBr_3$:PEO:$LiPF_6$ LEC/ITO devices. The inset shows the layering of In-Ga/$CsPbBr_3$:PEO:$LiPF_6$/ITO. e) Maximum luminance and power efficiency as a function of $LiPF_6$ concentration.

We first consider the distinct stages of LEC device operation, which are illustrated in Figures 1a-c. Initially, ions are uniformly distributed in the film (Figure 1a). In response to an applied bias,

cations drift toward and accumulate near the cathode, and anions likewise move toward and pack near the anode (Figure 1b). This leads to an electric double layer (EDL) formation at each electrode that induces higher electric fields, decreased width of the potential barriers (doping), and enhanced injection of electrons and holes that is insensitive to the workfunction of the electrodes (Figure 1c).[16-19] These injected carriers are transported through the bulk and radiatively recombine in the center of the device. The key features needed for successful LEC operation are therefore: 1) A sufficient concentration of mobile anions and cations; 2) Efficient transport of ions through the bulk for balanced EDL formation at the anode and cathode, leading to efficient charge injection; 3) Facile transport of electrons and holes through the semiconductor (which, for our system, requires a percolating network of the perovskite); 4) Efficient light emission upon recombination of the electrons and holes in the bulk, typically supported by a high quantum yield of the film. In our specific case, high luminescence efficiency is supported by the spectral properties of the $CsPbBr_3$ perovskite. To satisfy the other requirements, we introduce $LiPF_6$ salt, a salt that we have previously used to attain high performance in LECs utilizing ionic transition metal complexes.[20-22] (We have previously found that the lithium cation[20] and hexafluorophosphate anion[23] optimize device parameters.) We prepared films with an optimal concentration of the polymer electrolyte poly(ethylene oxide) (PEO) and systematically studied the effect of $LiPF_6$ salt addition.

The LECs were constructed with a single layer of spin cast perovskite film using an ITO anode, a $CsPbBr_3$:PEO:$LiPF_6$ perovskite composite (1:0.8 weight ratio $CsPbBr_3$:PEO, various $LiPF_6$ weight fractions), and an In-Ga eutectic cathode, as illustrated in the inset of Figure 1d (see Supporting Information Figure S1 and text for details of fabrication and testing). Also in Figure 1d, the current density versus voltage (J vs V) and luminance versus voltage (L vs V) graph of our devices with different ratios of $LiPF_6$ is shown. Figure 1e presents the maximum luminance and

power efficiency from the data of Figure 1d. All of the devices showed green electroluminescence centered near 528 nm with a FWHM of 20 nm (See Supporting information Figure S2). The reference device ($CsPbBr_3$:PEO with no $LiPF_6$) shows a turn-on voltage (V_{on}) of 2.5 V and a substantial maximum luminance of 8175 cd/m^2 at 5.5 V, with a maximum power efficiency of 1.6 Lm/W. This substantial luminance for a PeLEC is accounted for the optimized PEO electrolyte concentration within the film. As $LiPF_6$ is added into the $CsPbBr_3$:PEO film, the luminance and efficiency maxima increase gradually, peak at an optimal concentration, and then decrease. The best performance was achieved with a 0.5% $LiPF_6$ weight percentage, which showed a V_{on} of 1.9 V (below the bandgap), a maximum luminance of 14730 cd/m^2 at 5.4 V, and a maximum power efficiency of 3.0 Lm/W. Notably, the power efficiency (Figure 1e) was enhanced ~1.9X compared to the pristine $CsPbBr_3$:PEO LEC. Full performance metrics for all device formulations (Supporting Information Table S1), comparisons to other literature efforts (Supporting Information Table S3), and a detailed discussion of ionic redistribution is provided in the Supporting Information.

Further investigation of the devices reveals other key features. Turn on voltage is generally lowered by $LiPF_6$ addition, denoting its ability to assist in bipolar injection. Luminance is enhanced by adding 0.2% or 0.5% $LiPF_6$, but diminished by higher concentrations (Figure 1d), suggesting competing processes affect device performance. We also observe that the optimal 0.5% $LiPF_6$ concentration considerably reduces the hysteresis in current density curves from voltage cycling (Supporting Information Figure S3) and lowers the time for onset of emission (Supporting Information Figure S4), constistent with faster ionic redistribution. We also measured the stability of devices under constant voltage operation and found that 0.5% $LiPF_6$ can improve the stability threefold in comparison with control devices (Supporting Information Figure S4), a favorable

result in view of previous reports.[24] We performed additional study to gain further mechanistic and phenomenological understanding of these observations.

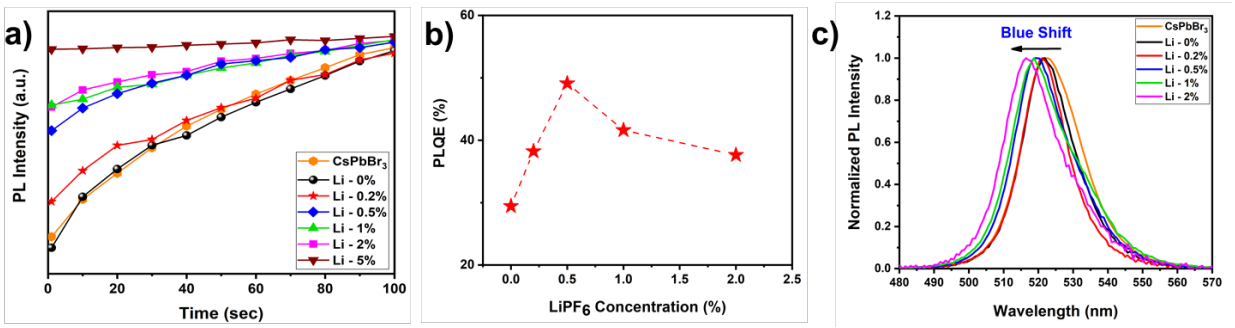

Figure 2. Photoluminescence properties of thin films of $CsPbBr_3$ and $CsPbBr_3$:PEO:$LiPF_6$ in air. a) Photoluminescence intensity as a function of time (λ_{ex}= 405 nm). b) Photoluminescence quantum efficiency (PLQE) versus $LiPF_6$ concentration for $CsPbBr_3$:PEO:$LiPF_6$ films in air. c) Photoluminescence spectra of $CsPbBr_3$ and $CsPbBr_3$:PEO:$LiPF_6$.

For further investigations of the optical, electronic, and morphological states of our perovskite films, we prepared $CsPbBr_3$:PEO:$LiPF_6$ thin films through an optimized one stage spin-coating process and vacuum treatment before annealing (Supporting Information Figure S5 and text). We subsequently measured the photoluminescence (PL) intensity versus time of these films (Figure 2a) in air. For $CsPbBr_3$ and $CsPbBr_3$:PEO films, the PL intensity dramatically increases with time. These PL dynamics have been observed in perovskite thin films and is associated with a carrier-assisted, oxygen-dependent trap deactivation reaction.[25-27] As $LiPF_6$ is added to $CsPbBr_3$:PEO films, the PL dynamic trends towards constant intensity. This PL trend with lithium addition can be understood from a reduced trap density.[28] In the absence of lithium salts, unfilled trap states are present, potentially due to grain boundaries, vacancies, and other imperfections that create nonradiative decay states in the middle of the optical gap. In air, these trap states must be deactivated before steady PL can be achieved. Lithium salt addition lowers the concentration of

these traps, leading to more stable PL. The oxygen dependence of this effect is confirmed by the lowering of the PL in nitrogen in Supporting Information Figure S6a. The morphological studies described below can further clarify the nature of trap suppression.

Time-resolved PL is also beneficial for observing the effects of lithium salts on trap suppression (Supporting Information Figure S6b). A $CsPbBr_3$:PEO film follows biexponential fluorescence decay with a significant fast (8.6 ns decay) and a smaller amplitude slower (36 ns) decay component. This fast component is likely associated with trapping states. Once $LiPF_6$ is added, the lifetimes follow a monoexponential decay with timescales of 20-30 ns. The suppression of the faster component is consistent with a reduced trap concentration.

To understand the influence of $LiPF_6$ addition on steady-state quantum yield, we measured the absolute photoluminescence quantum efficiency (PLQE) in air for $CsPbBr_3$:PEO:$LiPF_6$ films with an integrating sphere according to the methods described by de Mello *et al*. and Porrès *et al.*[29-30] Figure 2b reveals that the PLQE increases from 29% for a $CsPbBr_3$:PEO film to a maximum of 49% for a 0.5% $LiPF_6$ film of $CsPbBr_3$:PEO:$LiPF_6$, and then is lowered as the $LiPF_6$ concentration is further increased. This PLQE concentration trend of $CsPbBr_3$:PEO:$LiPF_6$ films qualitatively follows the concentration dependences of luminance and current efficiency for PeLEC devices (Figure 1e). Also, in Supporting Information S6a, PLQE is improved by over six fold between 0% and 0.5% $LiPF_6$ films when measured under nitrogen, where traps are not suppressed by oxygen. Furthermore, the relative change ($\Delta PLQE/PLQE_{air}$) between air (trap suppressing) and nitrogen (trap permitting) is lowered with $LiPF_6$ addition, correlating with lower trap concentration. This reinforces our assertion that $LiPF_6$ suppresses nonradiative trapping states to improve emission yield in thin films and devices.

PL spectra were also measured to ascertain the impact of lithium doping on optical emission from $CsPbBr_3$:PEO:$LiPF_6$ thin films (Figure 2c). The PL spectra show a gradual blue shift from λ_{max} = 522 nm for pure $CsPbBr_3$ thin film to λ_{max} = 516 nm for the $CsPbBr_3$:PEO:$LiPF_6$ (5%) thin film. Similar blueshifts and other spectral changes have been reported for Li, K, Sb, and Bi addition in perovskites and have been attributed to the Burstein-Moss effect and trap passivation.[14,31-33]

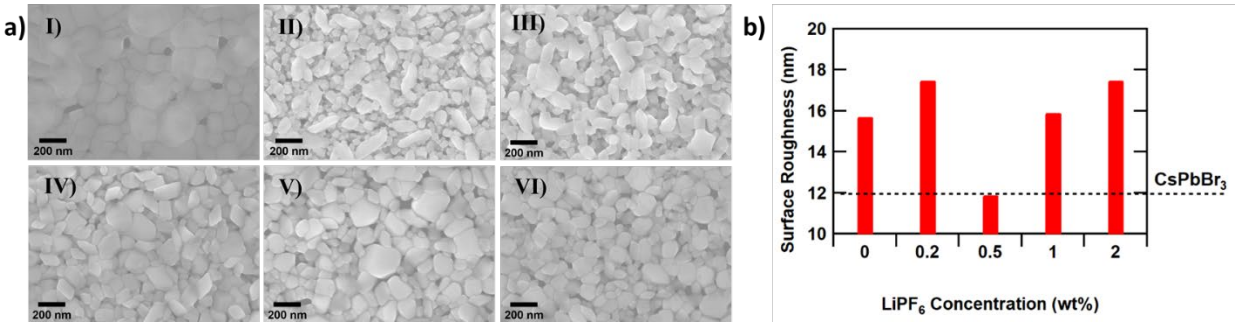

Figure 3. Morphological study of $CsPbBr_3$:PEO:$LiPF_6$ thin films by SEM and AFM. a) SEM for thin films of I) $CsPbBr_3$, II) $CsPbBr_3$:PEO, III) $CsPbBr_3$:PEO:$LiPF_6$ (0.2%), IV) $CsPbBr_3$:PEO:$LiPF_6$ (0.5%), V) $CsPbBr_3$:PEO:$LiPF_6$ (1%), and VI) $CsPbBr_3$:PEO:$LiPF_6$ (2%). b) Surface roughness of $CsPbBr_3$:PEO:$LiPF_6$ thin films versus $LiPF_6$ concentration as measured by AFM. The horizontal dotted line denotes the surface roughness of the pristine $CsPbBr_3$ film.

To further understand the morphological influence of the beneficial electrical and optical properties afforded by electrolyte and lithium addition, we studied thin perovskite films by scanning electron microscopy (SEM) and atomic force microscopy (AFM). The SEM image of the pristine $CsPbBr_3$ film (Figure 3a,I) reveals randomly oriented grains and substantial pinholes in the film. Addition of PEO (Figure 3a,II) reduces the average grain and pinhole sizes, but significant pinholes still remain. Subsequent addition of low concentrations ($\leq$ 2%) of $LiPF_6$ in $CsPbBr_3$:PEO increases the average grain size (Supporting Information Table S2) and decreases the number and

size of pinholes (Figure 3a, III-VI, Supporting Information Figure S7). The largest and most monodispersed grain sizes are observed for 0.5% and 1.0% $LiPF_6$ concentrations. Also, the 0.5% $LiPF_6$ dopant film (Figure 3a, IV) provides the most continuous network of perovskite crystals with the lowest amount of pinholes. This correlates well with the high luminance and efficiency of the 0.5% $LiPF_6$ doped LEC device (Figure 1e): reducing the number of pinholes limits detrimental leakage current, and the interpenetrating network of perovskite crystals supports facile transport of electrons and holes for efficient electroluminescence. On the other hand, excess $LiPF_6$ (5%) was detrimental to the quality of the thin film, leading to discontinuous films (Supporting Information Figure S8). This is likely due to the formation of lithium dendrites and subsequent phase separation.[34]

In Figure 3b, we relate the average surface roughness of the $CsPbBr_3$:PEO:$LiPF_6$ films with various percentages of $LiPF_6$ as measured by AFM (Supporting Information Figure S9). We observe a reduction in the root-mean-square roughness from 15.7 nm for the pristine $CsPbBr_3$:PEO film to 11.9 nm for the 0.5% $LiPF_6$ doped film, and an increase in surface roughness for higher concentrations. Again, this correlates with the optimal $LiPF_6$ device concentration, as low surface roughness improves the spatial uniformity of the electroluminescence and limits pinhole formation. Hence, the overall interpretation from SEM and AFM analysis indicates that 0.5% $LiPF_6$ corresponds to the optimal concentration for smooth films with large, percolating perovskite grains and minimal pinholes, all beneficial for superior device performance.

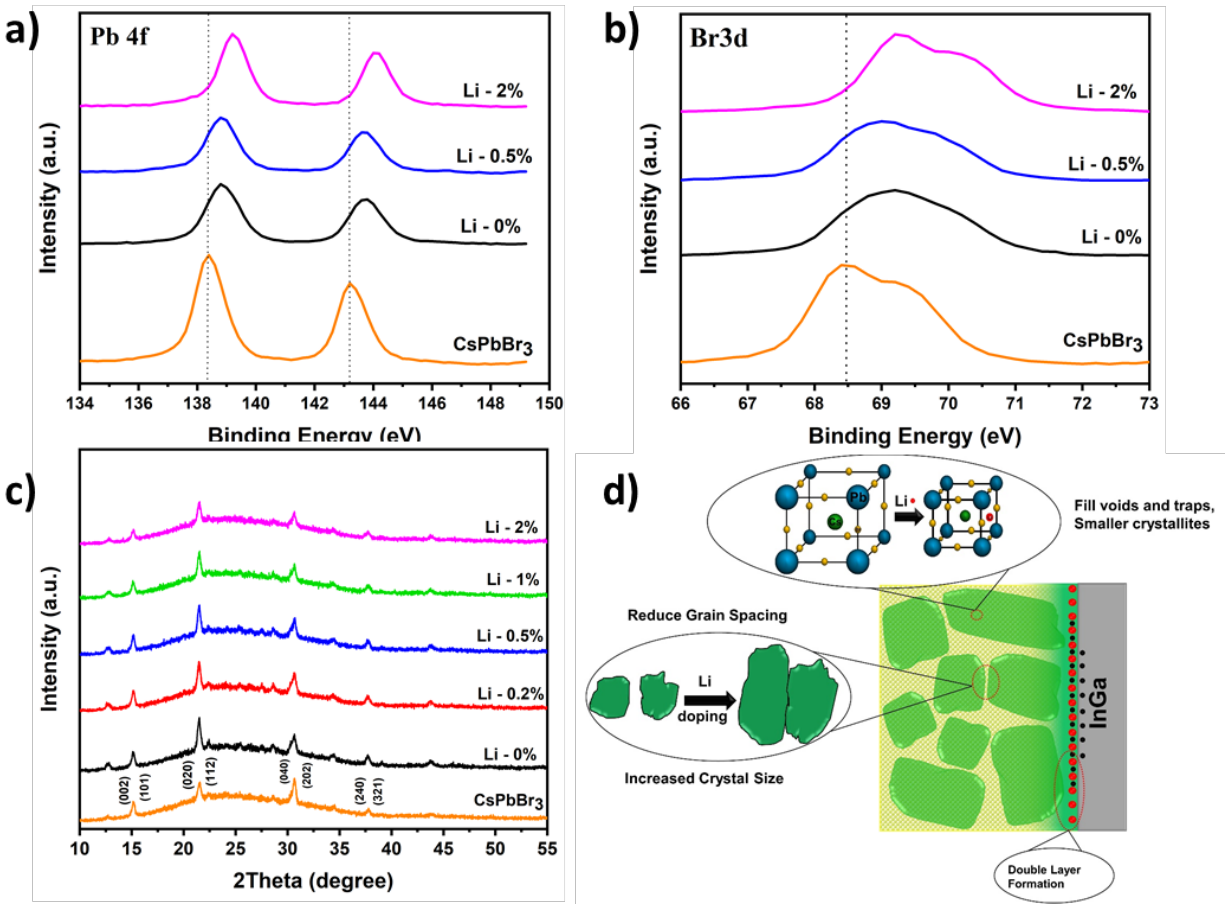

Figure 4. High resolution X-ray photoelectron spectroscopy (XPS) and X-ray diffraction (XRD) of $CsPbBr_3$:PEO:$LiPF_6$ films, as well as a conceptual illustration of Li^+-induced performance enhancement. High-resolution XPS spectral regions for a) Pb ($4f_{5/2}$, $4f_{7/2}$) and b) Br ($3d_{3/2}$, $3d_{5/2}$) peaks from $CsPbBr_3$ and $CsPbBr_3$:PEO:$LiPF_6$ thin films of various $LiPF_6$ weight ratios. c) XRD pattern of $CsPbBr_3$ and $CsPbBr_3$:PEO:$LiPF_6$ thin films of various $LiPF_6$ weight ratios. d) Conceptual illustration of the benefits afforded by $LiPF_6$ doping in PeLECs.

X-ray photoelectron spectroscopy (XPS) analysis of the high resolution spectra involving Pb 4f, Br 3d, C 1s, and F 1s (Figure 4a-b, and Supporting Information Figure S10) was conducted to further understand the effect of the $LiPF_6$ dopant in $CsPbBr_3$:PEO films. As shown in Figure 4a, the Pb 4f spectrum for the pristine $CsPbBr_3$ film has two peaks associated with $4f_{5/2}$ and $4f_{7/2}$

orbitals located at 138.40 and 143.20 eV, respectively, which correspond to Pb^{2+} cations. The two Br 3d signals, corresponding to $3d_{3/2}$ and $3d_{5/2}$ peaks, are also clearly seen at 68.4 and 69.2 eV. Addition of PEO to the $CsPbBr_3$ film shifts all of these peaks to higher binding energies, which is attributed to the interaction between PEO and metallic/ion Pb reported previously.[35] Furthermore, we also observe that adding $LiPF_6$ dopant to the $CsPbBr_3$:PEO film further shifts these peaks. These spectral shifts are a clear indication of a lattice contraction of perovskite after Li^+ incorporation, shorter Pb-Br bonds and higher binding energy for Pb 4f and Br 3d.[28,36] The presence of PEO and $LiPF_6$ in films has been further confirmed from the C 1s and F 1s XPS spectra (Supporting Information Figure S10a-b). The adventitious C 1s signal is obvious at 285.2 eV for the pristine $CsPbBr_3$ thin film. However, after PEO addition, a new C 1s peak appears at 287 eV, which corresponds to the C-O-C groups of the PEO.[37] An F 1s spectral peak at 686.6 eV appears after adding $LiPF_6$ to $CsPbBr_3$:PEO, confirming the presence of the fluoride ion in the film. Also, we note that the photoemission of Li 1s could not be detected due to the very low sensitivity factor of Li. The detailed chemical bonding of the composite perovskite films was analyzed by deconvoluting the XPS peaks (Supporting Information Figure S10).

Figure 4c illustrates the X-ray diffraction (XRD) spectra of $CsPbBr_3$, $CsPbBr_3$:PEO, and $CsPbBr_3$:PEO:$LiPF_6$. The thin film XRD spectra indicate the primary diffraction peaks at 15.21°, 21.46°, and 30.70° that corresponds to diffraction planes of (110), (112) and (220), respectively, in agreement with previous reports for an orthorhombic (Pnma) crystal structure.[38-39] The peaks at 12.7° and 22.41° indicate the presence of a trigonal phase of Cs_4PbBr_6 with the diffraction planes of (102) and (213), respectively, as seen in literature, indicating a mixed phase of $CsPbBr_3$ and Cs_4PbBr_6.[40-42] In addition, we analyzed the peak widths, finding successive contraction of the perovskite crystallite size from 16.5-17.0 nm to 13.0-13.2 nm with increasing amounts of $LiPF_6$

(see Supporting Information Table S2). This is consistent with experimental and computational observations that lithium ions occupy interstitial sites and stabilize the lattice.[43]

Overall, these observations suggest several benefits of lithium salt addition that led to high luminance (14730 cd/m^2) among single layer PeLECs that is comparable to high performance PeLEDs, which are typically multilayer devices (Supporting Information Table S3). These benefits are summarized in Figure 4d. First, an overall consideration of the system and a detailed view of the device performance suggests that an optimal concentration of $LiPF_6$ facilitates double layer formation, thus improving charge carrier injection. Second, SEM and AFM studies demonstrated that an optimal lithium concentration reduces the spacing between grain boundaries, leading to smooth, pinhole free films. This limits leakage current, enables high electron and hole conductivities for enhanced carrier transport. PL study correlated with XPS and XRD studies show that lithium reduces the crystallite size through filling traps and voids, reducing sources of nonradiative losses for highly efficient light emission in thin films and devices. A detailed balance of all of these features thus leads to high performance LECs of simple, single-layer architectures for next generation optoelectronic applications.

ASSOCIATED CONTENT

Supporting information available: experimental methods, electroluminescence spectra, current and luminance versus voltage and time, efficiency metrics, capacitance versus frequency, time-resolved PL measurements, PL quantum efficiency in air and nitrogen, SEM and AFM images, XPS spectra, XRD data, illustrations of film formation and ion accumulation, discussion of ionic redistribution.

ACKNOWLEDGMENT

J.D.S. acknowledges support from the National Science Foundation (ECCS 1906505). Q.G. acknowledges support from the Welch Foundation (AT-1992-20190330). A.Z. acknowledges support from the Welch Foundation (AT-1617) and from the Ministry of Education and Science of the Russian Federation (14.Y26.31.0010). A.I. also thanks financial support of Russian Federation grants No K2-2019-014 in NUST MISIS and 14.Y26.31.0010 in ITMO University. We would also like to thank Siqing Li for assistance with the time-resolved PL measurements.

References

1. Song, J. Z.; Xu, L. M.; Li, J. H.; Xue, J.; Dong, Y. H.; Li, X. M.; Zeng, H. B., Monolayer and Few-Layer All-Inorganic Perovskites as a New Family of Two-Dimensional Semiconductors for Printable Optoelectronic Devices. *Adv. Mater.* **2016,** *28* (24), 4861-4869.

2. Dong, Y. H.; Gu, Y.; Zou, Y. S.; Song, J. Z.; Xu, L. M.; Li, J. H.; Xue, F.; Li, X. M.; Zeng, H. B., Improving All-Inorganic Perovskite Photodetectors by Preferred Orientation and Plasmonic Effect. *Small* **2016,** *12* (40), 5622-5632.

3. Ling, Y. C.; Tian, Y.; Wang, X.; Wang, J. C.; Knox, J. M.; Perez-Orive, F.; Du, Y. J.; Tan, L.; Hanson, K.; Ma, B. W.; Gao, H. W., Enhanced Optical and Electrical Properties of Polymer-Assisted All-Inorganic Perovskites for Light-Emitting Diodes. *Adv. Mater.* **2016,** *28* (40), 8983-8989.

4. Kim, Y. H.; Lee, G. H.; Kim, Y. T.; Wolf, C.; Yun, H. J.; Kwon, W.; Park, C. G.; Lee, T. W., High Efficiency Perovskite Light-Emitting Diodes of Ligand-Engineered Colloidal Formamidinium Lead Bromide Nanoparticles. *Nano Energy* **2017,** *38*, 51-58.

5. Zhang, L. Q.; Yang, X. L.; Jiang, Q.; Wang, P. Y.; Yin, Z. G.; Zhang, X. W.; Tan, H. R.; Yang, Y.; Wei, M. Y.; Sutherland, B. R.; Sargent, E. H.; You, J. B., Ultra-bright and Highly Efficient Inorganic Based Perovskite Light-Emitting Diodes. *Nat. Commun.* **2017,** *8*, 15640.

6. Xiao, Z. G.; Kerner, R. A.; Zhao, L. F.; Tran, N. L.; Lee, K. M.; Koh, T. W.; Scholes, G. D.; Rand, B. P., Efficient Perovskite Light-Emitting Diodes Featuring Nanometre-Sized Crystallites. *Nat. Photonics* **2017,** *11* (2), 108-115.

7. Kim, Y. H.; Wof, C.; Kim, Y. T.; Cho, H.; Kwon, W.; Do, S.; Sadhanala, A.; Park, C. G.; Rhee, S. W.; Im, S. H.; Friend, R. H.; Leet, T. W., Highly Efficient Light-Emitting Diodes of Colloidal Metal-Halide Perovskite Nanocrystals beyond Quantum Size. *ACS Nano* **2017,** *11* (7), 6586-6593.

8. Xu, W. D.; Hu, Q.; Bai, S.; Bao, C. X.; Miao, Y. F.; Yuan, Z. C.; Borzda, T.; Barker, A. J.; Tyukalova, E.; Hu, Z. J.; Kawecki, M.; Wang, H. Y.; Yan, Z. B.; Liu, X. J.; Shi, X. B.; Uvdal, K.; Fahlman, M.; Zhang, W. J.; Duchamp, M.; Liu, J. M.; Petrozza, A.; Wang, J. P.; Liu, L. M.; Huang, W.; Gao, F., Rational molecular passivation for high-performance perovskite light-emitting diodes. *Nat. Photonics* **2019,** *13* (6), 418-426.

9. Lin, K. B.; Xing, J.; Quan, L. N.; de Arquer, F. P. G.; Gong, X. W.; Lu, J. X.; Xie, L. Q.; Zhao, W. J.; Zhang, D.; Yan, C. Z.; Li, W. Q.; Liu, X. Y.; Lu, Y.; Kirman, J.; Sargent, E. H.; Xiong, Q. H.; Wei, Z. H., Perovskite light-emitting diodes with external quantum efficiency exceeding 20 per cent. *Nature* **2018,** *562* (7726), 245-248.

10. Cho, H. C.; Jeong, S. H.; Park, M. H.; Kim, Y. H.; Wolf, C.; Lee, C. L.; Heo, J. H.; Sadhanala, A.; Myoung, N.; Yoo, S.; Im, S. H.; Friend, R. H.; Lee, T. W., Overcoming the

electroluminescence efficiency limitations of perovskite light-emitting diodes. *Science* **2015,** *350* (6265), 1222-1225.

11. Ayguler, M. F.; Weber, M. D.; Puscher, B. M. D.; Medina, D. D.; Docampo, P.; Costa, R. D., Light-Emitting Electrochemical Cells Based on Hybrid Lead Halide Perovskite Nanoparticles. *J. Phys. Chem. C* **2015,** *119* (21), 12047-12054.

12. Zhang, H. M.; Lin, H.; Liang, C. J.; Liu, H.; Liang, J. J.; Zhao, Y.; Zhang, W. G.; Sun, M. J.; Xiao, W. K.; Li, H.; Polizzi, S.; Li, D.; Zhang, F. J.; He, Z. Q.; Choy, W. C. H., Organic-Inorganic Perovskite Light-Emitting Electrochemical Cells with a Large Capacitance. *Adv. Funct. Mater.* **2015,** *25* (46), 7226-7232.

13. Puscher, B. M. D.; Ayguler, M. F.; Docampo, P.; Costa, R. D., Unveiling the Dynamic Processes in Hybrid Lead Bromide Perovskite Nanoparticle Thin Film Devices. *Adv. Energy Mater.* **2017,** *7* (15), 1602283.

14. Ayguler, M. F.; Puscher, B. M. D.; Tong, Y.; Bein, T.; Urban, A. S.; Costa, R. D.; Docampo, P., Light-Emitting Electrochemical Cells Based on Inorganic Metal Halide Perovskite Nanocrystals. *J. Phys. D-Appl. Phys.* **2018,** *51* (33), 334001.

15. Andricevic, P.; Mettan, X.; Kollar, M.; Nafradi, B.; Sienkiewicz, A.; Garma, T.; Rossi, L.; Forro, L.; Horvath, E., Light-Emitting Electrochemical Cells of Single Crystal Hybrid Halide Perovskite with Vertically Aligned Carbon Nanotubes Contacts. *ACS Photonics* 2019, 6 (4), 967-975.

16. Pei, Q. B.; Yu, G.; Zhang, C.; Yang, Y.; Heeger, A. J., Polymer Light-Emitting Electrochemical Cells. *Science* **1995,** *269* (5227), 1086-1088.

17. de Mello, J. C., Interfacial Feedback Dynamics in Polymer Light-Emitting Electrochemical Cells. *Phys. Rev. B* **2002,** *66* (23), 235210.

18. Costa, R. D.; Orti, E.; Bolink, H. J.; Monti, F.; Accorsi, G.; Armaroli, N., Luminescent Ionic Transition-Metal Complexes for Light-Emitting Electrochemical Cells. *Angew. Chem.-Int. Edit.* **2012,** *51* (33), 8178-8211.

19. Slinker, J. D.; DeFranco, J. A.; Jaquith, M. J.; Silveira, W. R.; Zhong, Y.-W.; Moran-Mirabal, J. M.; Craighead, H. G.; Abruna, H. D.; Marohn, J. A.; Malliaras, G. G., Direct Measurement of the Electric-Field Distribution in a Light-Emitting Electrochemical Cell. *Nat. Mater.* **2007,** *6* (11), 894-899.

20. Shen, Y.; Kuddes, D. D.; Naquin, C. A.; Hesterberg, T. W.; Kusmierz, C.; Holliday, B. J.; Slinker, J. D., Improving Light-Emitting Electrochemical Cells with Ionic Additives. *Appl. Phys. Lett.* **2013,** *102* (20), 203305.

21. Bastatas, L. D.; Lin, K. Y.; Moore, M. D.; Suhr, K. J.; Bowler, M. H.; Shen, Y. L.; Holliday, B. J.; Slinker, J. D., Discerning the Impact of a Lithium Salt Additive in Thin-Film Light-Emitting Electrochemical Cells with Electrochemical Impedance Spectroscopy. *Langmuir* **2016,** *32* (37), 9468-9474.

22. Suhr, K. J.; Bastatas, L. D.; Shen, Y. L.; Mitchell, L. A.; Holliday, B. J.; Slinker, J. D., Enhanced Luminance of Electrochemical Cells with a Rationally Designed Ionic Iridium Complex and an Ionic Additive. *ACS Appl. Mater. Interfaces* **2016,** *8* (14), 8888-8892.

23. Bastatas, L. D.; Moore, M. D.; Slinker, J. D., The Effect of the Dielectric Constant and Ion Mobility in Light-Emitting Electrochemical Cells. *ChemPlusChem* **2018**, *83* (4), 266-273.

24. Li, J. Q.; Shan, X.; Bade, S. G. R.; Geske, T.; Jiang, Q. L.; Yang, X.; Yu, Z. B., Single-Layer Halide Perovskite Light-Emitting Diodes with Sub-Band Gap Turn-On Voltage and High Brightness. *J. Phys. Chem. Lett.* **2016,** *7* (20), 4059-4066.

25. Galisteo-Lopez, J. F.; Anaya, M.; Calvo, M. E.; Miguez, H., Environmental Effects on the Photophysics of Organic-Inorganic Halide Perovskites. *J. Phys. Chem. Lett.* **2015,** *6* (12), 2200-2205.

26. Tian, Y. X.; Peter, M.; Unger, E.; Abdellah, M.; Zheng, K.; Pullerits, T.; Yartsev, A.; Sundstrom, V.; Scheblykin, I. G., Mechanistic insights into perovskite photoluminescence enhancement: light curing with oxygen can boost yield thousandfold. *Phys. Chem. Chem. Phys.* **2015,** *17* (38), 24978-24987.

27. Fu, X.; Jacobs, D. A.; Beck, F. J.; Duong, T.; Shen, H. P.; Catchpole, K. R.; White, T. P., Photoluminescence study of time- and spatial-dependent light induced trap de-activation in $CH_3NH_3PbI_3$ perovskite films. *Phys. Chem. Chem. Phys.* **2016,** *18* (32), 22557-22564.

28. Fang, Z. S.; He, H. P.; Gan, L.; Li, J.; Ye, Z. Z., Understanding the Role of Lithium Doping in Reducing Nonradiative Loss in Lead Halide Perovskites. *Adv. Sci.* **2018,** *5* (12), 1800736.

29. de Mello, J. C.; Wittmann, H. F.; Friend, R. H., An Improved Experimental Determination of External Photoluminescence Quantum Efficiency. *Adv. Mater.* **1997,** *9* (3), 230-232.

30. Porres, L.; Holland, A.; Palsson, L. O.; Monkman, A. P.; Kemp, C.; Beeby, A., Absolute Measurements of Photoluminescence Quantum Yields of Solutions Using an Integrating Sphere. *J. Fluoresc.* **2006,** *16* (2), 267-272.

31. Jiang, Q. L.; Chen, M. M.; Li, J. Q.; Wang, M. C.; Zeng, X. Q.; Besara, T.; Lu, J.; Xin, Y.; Shan, X.; Pan, B. C.; Wang, C. C.; Lin, S. C.; Siegrist, T.; Xiao, Q. F.; Yu, Z. B., Electrochemical Doping of Halide Perovskites with Ion Intercalation. *ACS Nano* **2017,** *11* (1), 1073-1079.

32. Zhang, J.; Shang, M. H.; Wang, P.; Huang, X. K.; Xu, J.; Hu, Z. Y.; Zhu, Y. J.; Han, L. Y., n-Type Doping and Energy States Tuning in $CH_3NH_3Pb_{1-x}Sb_{2x/3}I_3$ Perovskite Solar Cells. *ACS Energy Lett.* **2016,** *1* (3), 535-541.

33. Begum, R.; Parida, M. R.; Abdelhady, A. L.; Murali, B.; Alyami, N. M.; Ahmed, G. H.; Hedhili, M. N.; Bakr, O. M.; Mohammed, O. F., Engineering Interfacial Charge Transfer in $CsPbBr_3$ Perovskite Nanocrystals by Heterovalent Doping. *J. Am. Chem. Soc.* **2017,** *139* (2), 731-737.

34. Niu, S. A.; Cao, Z.; Li, S.; Yan, T. Y., Structure and Transport Properties of the LiPF6 Doped 1-Ethyl-2,3-dimethyl-imidazolium Hexaftuorophosphate Ionic Liquids: A Molecular Dynamics Study. *J. Phys. Chem. B* **2010,** *114* (2), 877-881.

35. Yu, H. T.; Lu, Y.; Feng, Z. Q.; Wu, Y. A.; Liu, Z. W.; Xia, P. F.; Qian, J.; Chen, Y. F.; Liu, L. H.; Cao, K.; Chen, S. F.; Huang, W., A MAPbBr(3):poly(ethylene oxide) composite perovskite quantum dot emission layer: enhanced film stability, coverage and device performance. *Nanoscale* **2019,** *11* (18), 9103-9114.

36. Liu, M.; Zhong, G. H.; Yin, Y. M.; Miao, J. S.; Li, K.; Wang, C. Q.; Xu, X. R.; Shen, C.; Meng, H., Aluminum-Doped Cesium Lead Bromide Perovskite Nanocrystals with Stable Blue Photoluminescence Used for Display Backlight. *Adv. Sci.* **2017,** *4* (11), 1700335.

37. Chan, C. M.; Weng, L. T., Surface Characterization of Polymer Blends by XPS and ToF-SIMS. *Materials* **2016,** *9* (8), 655.

38. Yantara, N.; Bhaumik, S.; Yan, F.; Sabba, D.; Dewi, H. A.; Mathews, N.; Boix, P. P.; Demir, H. V.; Mhaisalkar, S., Inorganic Halide Perovskites for Efficient Light-Emitting Diodes. *J. Phys. Chem. Lett.* **2015,** *6* (21), 4360-4364.

39. Zhang, M. Z.; Zheng, Z. P.; Fu, Q. Y.; Chen, Z.; He, J. L.; Zhang, S.; Yan, L.; Hu, Y. X.; Luo, W., Growth and Characterization of All-Inorganic Lead Halide Perovskite Semiconductor $CsPbBr_3$ Single Crystals. *CrystEngComm* **2017,** *19* (45), 6797-6803.

40. Zhang, H. H.; Liao, Q.; Wu, Y. S.; Chen, J. W.; Gao, Q. G.; Fu, H. B., Pure Zero-Dimensional Cs_4PbBr_6 Single Crystal Rhombohedral Microdisks with High Luminescence and Stability. *Phys. Chem. Chem. Phys.* **2017,** *19* (43), 29092-29098.

41. Lou, S. Q.; Zhou, Z.; Xuan, T. T.; Li, H. L.; Jiao, J.; Zhang, H. W.; Gautier, R.; Wang, J., Chemical Transformation of Lead Halide Perovskite into Insoluble, Less Cytotoxic, and Brightly Luminescent $CsPbBr_3/CsPb_2Br_5$ Composite Nanocrystals for Cell Imaging. *ACS Appl. Mater. Interfaces* **2019,** *11* (27), 24241-24246.

42. Chen, Y. M.; Zhou, Y.; Zhao, Q.; Zhang, J. Y.; Ma, J. P.; Xuan, T. T.; Guo, S. Q.; Yong, Z. J.; Wang, J.; Kuroiwa, Y.; Moriyoshi, C.; Sun, H. T., $Cs_4PbBr_6/CsPbBr_3$ Perovskite Composites with Near-Unity Luminescence Quantum Yield: Large-Scale Synthesis, Luminescence and Formation Mechanism, and White Light-Emitting Diode Application. *ACS Appl. Mater. Interfaces* **2018,** *10* (18), 15905-15912.

43. Cao, J.; Tao, S. X.; Bobbert, P. A.; Wong, C. P.; Zhao, N., Interstitial Occupancy by Extrinsic Alkali Cations in Perovskites and Its Impact on Ion Migration. *Adv. Mater.* **2018,** *30* (26), 1707350.

Supporting Information

Bright and Effectual Perovskite Light Emitting Electrochemical Cells Leveraging Ionic Additives

Masoud Alahbakhshi[1], Aditya Mishra[2], Ross Haroldson[3], Arthur Ishteev[5,6], Jiyoung Moon[2], Qing Gu[1], Jason D. Slinker[2,3] and Anvar A. Zakhidov[3,4,5,6]**

[1]Department of Electrical and Computer Engineering, The University of Texas at Dallas, 800 West Campbell Road, Richardson, Texas 75080-3021, United States.

[2]Department of Materials Science and Engineering, The University of Texas at Dallas, 800 West Campbell Road, Richardson, Texas 75080-3021, United States.

[3]Department of Physics, The University of Texas at Dallas, 800 West Campbell Road, Richardson, Texas 75080-3021, United States.

[4]NanoTech Institute, The University of Texas at Dallas, 800 West Campbell Road, Richardson, Texas 75080-3021, United States.

[5]Department of Nanophotonics and Metamaterials, ITMO University, St. Petersburg, Moscow, Russia.

[6]Laboratory of Advanced Solar Energy, NUST MISiS, Moscow, 119049, Russia

Experimental Methods

Figures and Tables

Experimental Methods

Materials: Lead (II) bromide ($PbBr_2$; 99.99% trace metal basis), Cesium bromide (CsBr; 99.99%) and Polyethylene Oxide (PEO; M.W. > 5,000,000) were all purchased from Alfa Aesar. Lithium Hexafluorophosphate ($LiPF_6$; 99.99%) and Dimethyl Sulfoxide (DMSO; anhydrous > 99.9 %) were purchased from Sigma Aldrich. Gallium Indium eutectic (GaIn; 99.99%) was purchased from Beantown Chemical.

Perovskite Solution Preparation: The $CsPbBr_3$-based precursor solution was prepared by dissolving $PbBr_2$ and CsBr in a 1:1.5 molar ratio with PEO (10 mg/ml) in anhydrous DMSO solution. Then the perovskite precursor solution was stirred at 60 °C for dissolution overnight. When all solutions were dissolved, an empty vial was weighed and the desirable amount of PEO was added, then the weight difference before and after the PEO addition was measured to get an accurate weight of the viscous solution. The weight ratio of $CsPbBr_3$ to PEO was 100:80. Finally, these solutions were blended with 4 mg/ml DMSO solutions of $LiPF_6$ to prepare mixtures of five different weight ratios (0.2%, 0.5%, 1%, 2% and 5%) of lithium salt with the perovskite-polymer composition.

Device Fabrication: The ITO/glass substrates (Liasion Quartz (Lianyungang Jiangsu China), sheet resistance ~ 15 Ω sq^{-1}) were cleaned sequentially with detergent solution, deionized water, acetone, Toluene and 2-propanol in an ultra-sonication bath for 15 mins. Subsequently, the

substrates were dried with nitrogen and treated for 20 min with UV-ozone. To obtain $CsPbBr_3$:PEO:$LiPF_6$ thin films, precursor solutions were spin-coated onto ITO substrates at 1200 rpm for 45 min. Then, the thin film was put under vacuum for 1 minute to have a uniform and pinhole-free thin film. Finally, the $CsPbBr_3$:PEO:$LiPF_6$ film was annealed at 150 °C for 15 seconds to remove the residual solvent. An InGa top electrode was deposited on the film as a droplet using a syringe (Figure S1) and the LEC device is lowered into contact with the InGa droplet. The device area (3.1 mm^2) was measured by calibrating the image size observed in a spectroradiometer.

Electroluminescence Measurements: All measurements were conducted using a mechanical probe-station under high vacuum <10mTorr. Current density-voltage (J-V) and luminance-voltage (L-V) characteristics were measured using a Keithley 236 source meter and a Photo Research PR-650 spectroradiometer in the range of 0V to 6V with a 0.3V increment. Additional current-only measurements were taken with a Keithley 2400 in a nitrogen glove box environment.

Photoluminescence *vs* Time Measurements: Measurements were taken using an Ocean Optics QE65000 spectrometer coupled with a fiber optic cable pointed at the thin films through a 450nm longpass dielectric filter to block out the 405nm CW laser diode excitation signal.

Photoluminescence Quantum Efficiency Measurements: Thin film samples deposited on glass were attached to a custom holder then placed inside a Spectral Physics integrating sphere. Samples were excited at a 15 degree angle incidence to avoid back reflecting excitation light out of the integrating sphere. Using the method developed by de Mello *et al*., we took measurements of the excited thin films both in and out of the excitation beam path [1]. Fluctuations in excitation power were monitored by splitting the beam with a beam splitter and placing a photodiode power meter hooked up to a Thorlabs PDA200C photodiode amplifier. The collimated beam profile was shaped

with a precision cut 1000 micron diameter circular aperture. The power density was then measured to be 561±4 mW/cm^2. A fiber optic cable was mounted to one of the integrating sphere ports and was coupled to the Ocean Optics QE65000 spectrometer where spectrum measurements were taken.

Scanning Electron Microscopy (SEM): Secondary electron SEM images were taken with a Zeiss Supra-40 SEM using an in-lens detector at an accelerating voltage of 10kV.

Atomic Force Microscopy (AFM): The AFM images were performed using a Veeco Model 3100 Dimension V to scrutinize the morphology of thin films. The thin films were scanned for 5μm × 5μm area at 0.8Hz rate using an OTESPA-R3 AFM tip from Bruker. Tapping mode AFM was used for this characterization.

X-ray Photoelectron Spectroscopy (XPS): XPS measurements were conducted on perovskite thin films using a Versa Probe II at an ultrahigh vacuum of 10^{-8} Pa. The X-ray source was an Al Kα which has 1486.6eV photon energy, 50W gun power, 15kV operating voltage, 200um X-ray spot size, and 59° angle between the X-ray source and detector. The calibration using internal standard Au, Cu, and Ag samples was performed before obtaining the XPS data. Data was collected without injecting a flux of low energy electrons.

X-Ray Diffraction (XRD): XRD measurements were collected using a Rigaku SmartLab X-ray Cu target (Ka1=1.54059 Å) and a HyPix 3000 detector. The 2-theta/omega scan was consistently performed in the 2-theta range of 10° to 55° with a 0.01° step and a ~1°/min scan speed.

Supporting Information Figure S1

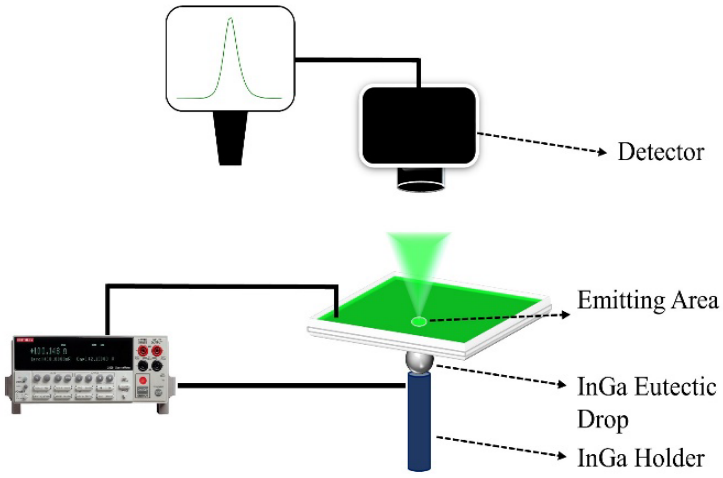

Figure S1. The experimental setup for capturing the electroluminescence performance of In-Ga/$CsPbBr_3$:PEO:$LiPF_6$/ITO LEC devices.

Supporting Information Figure S2

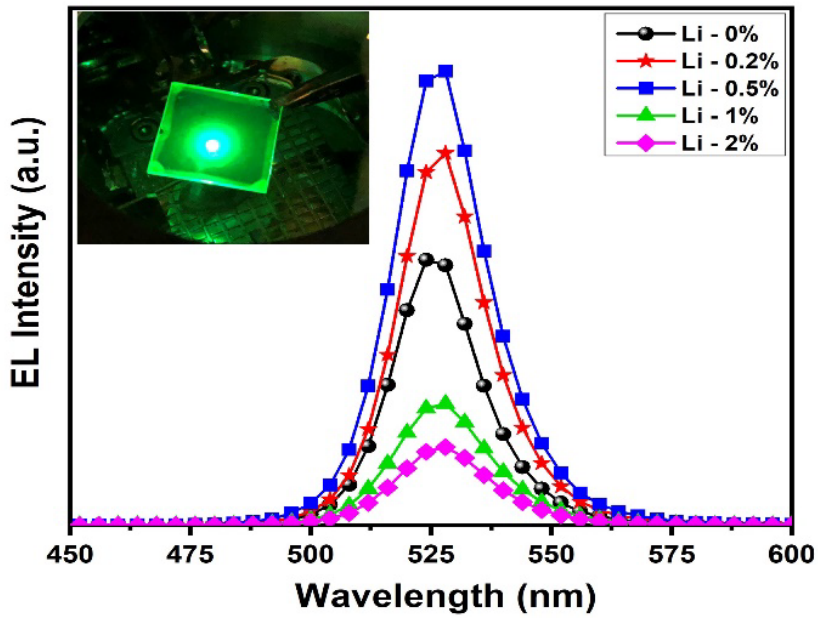

Figure S2. Electroluminescence spectra of In-Ga/$CsPbBr_3$:PEO:$LiPF_6$/ITO light emitting electrochemical cells with various weight ratios of $LiPF_6$. The inset shows the electroluminescence of a 0.5% $LiPF_6$ PeLEC operating at 5 volts.

Supporting Information Table S1

Table S1. Summrized performance of In-Ga/$CsPbBr_3$:PEO:$LiPF_6$/ITO LEC devices with different ratios of $LiPF_6$.

Devices	Turn-on Voltage (V)	Max Current Efficiency (cd/A)	Max Luminance (cd/m^2)	Max External Quantum Efficiency (%)	Max Power Efficiency (Lm/W)
$CsPbBr_3$:PEO (0%)	2.5	1.5	8175	0.38	1.6
$CsPbBr_3$:PEO:$LiPF_6$ (0.2%)	2.2	1.4	11800	0.34	1.6
$CsPbBr_3$:PEO:$LiPF_6$ (0.5%)	1.9	2.8	14730	0.71	3.0
$CsPbBr_3$:PEO:$LiPF_6$ (1%)	2.4	2.2	5675	0.55	2.5
$CsPbBr_3$:PEO:$LiPF_6$ (2%)	2.4	1.0	2619	0.25	1.0
$CsPbBr_3$:PEO:$LiPF_6$ (5%)	2.7	1.8	177	0.50	1.9

Supporting Information Figure S3

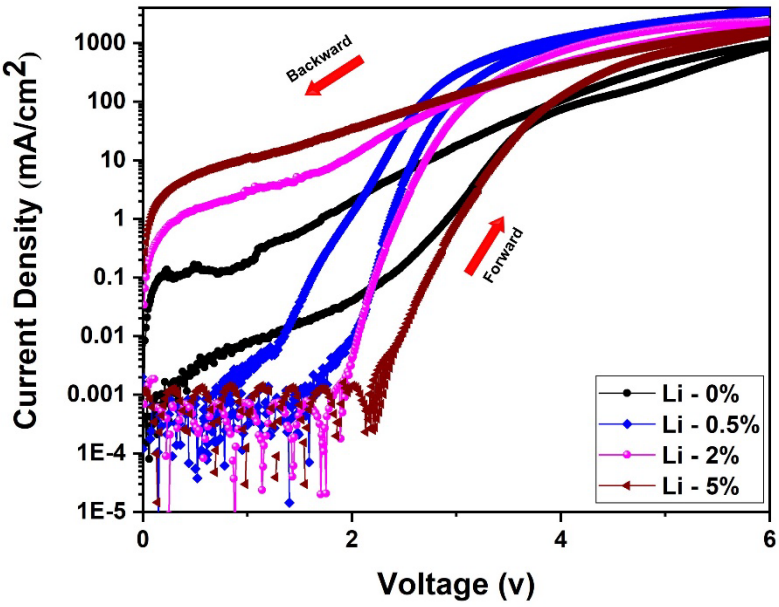

Figure S3. Current density versus voltage of In-Ga/$CsPbBr_3$:PEO:$LiPF_6$/ITO LEC devices with different ratios of $LiPF_6$. The graph clearly shows that in the optimized ratio of Li (0.5%), the hysteresis state decreases significantly.

Supporting Information Figure S4

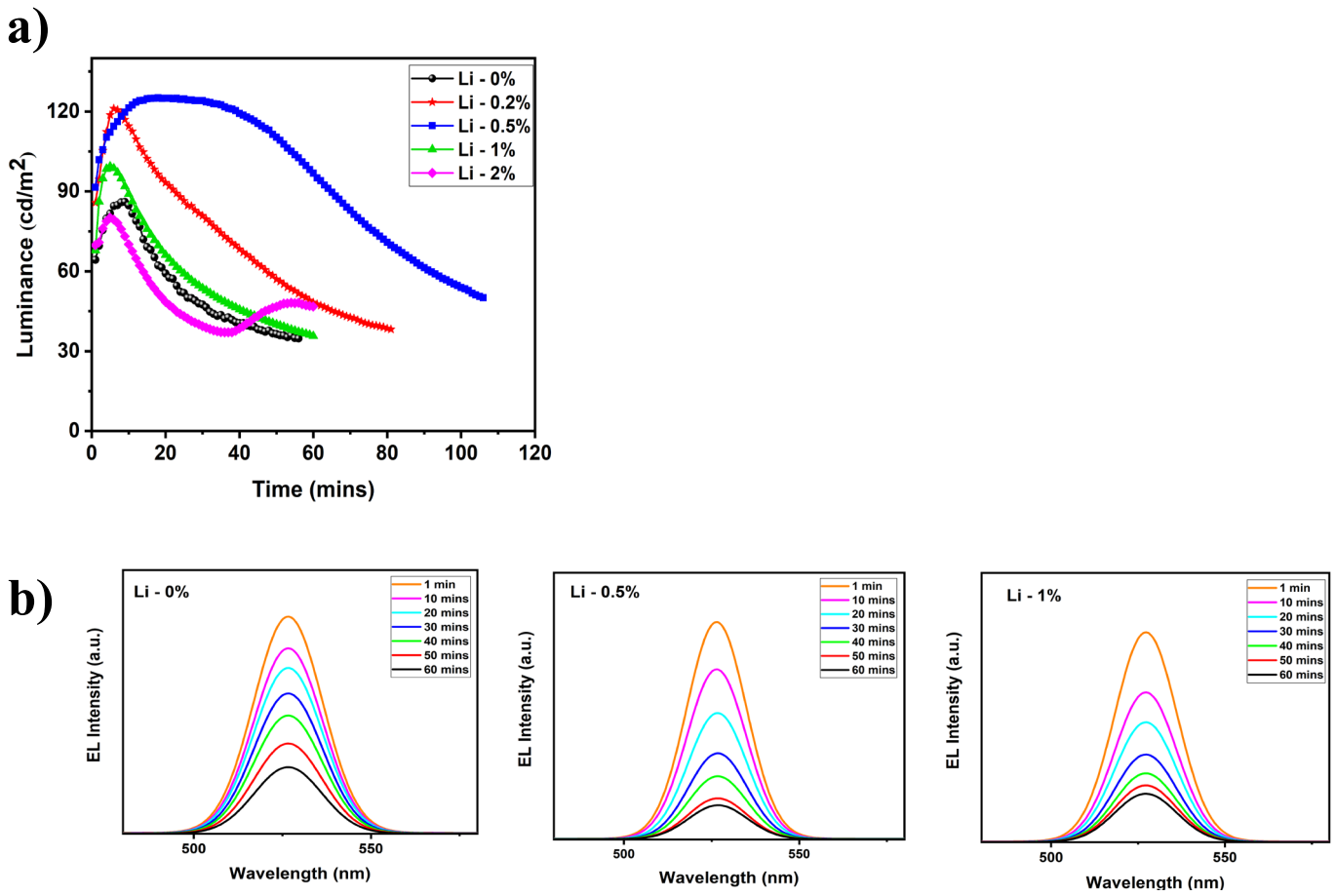

Figure S4. a) Luminance versus time for constant voltage operation of In-Ga/$CsPbBr_3$:PEO:$LiPF_6$/ITO LEC devices with different ratios of $LiPF_6$, demonstrating increased stability with optimal $LiPF_6$ concentration. b) EL spectrum changing of Li-0% , Li-0.5% and Li-1% devices in time. The results show that there is no any shifts in different ratio of $LiPF_6$

Supporting Information Figure S5

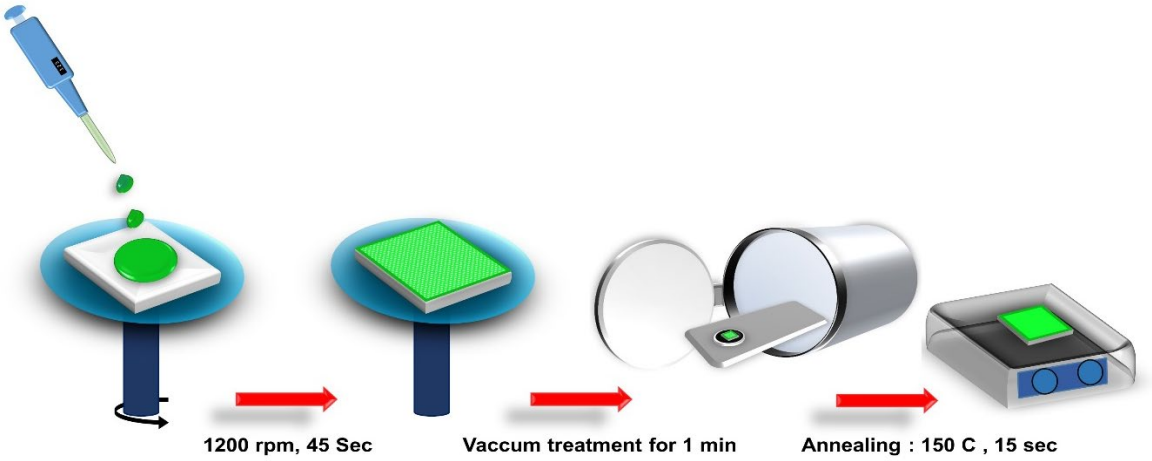

Figure S5. Illustration of the fabrication of thin films of $CsPbBr_3$:PEO:$LiPF_6$. Initially, components are spin cast at 1200 rpm for 45 seconds, followed by rapid vacuum treatment for 1 minute and annealing for 15 seconds at 115 °C.

Supporting Information Figure S6

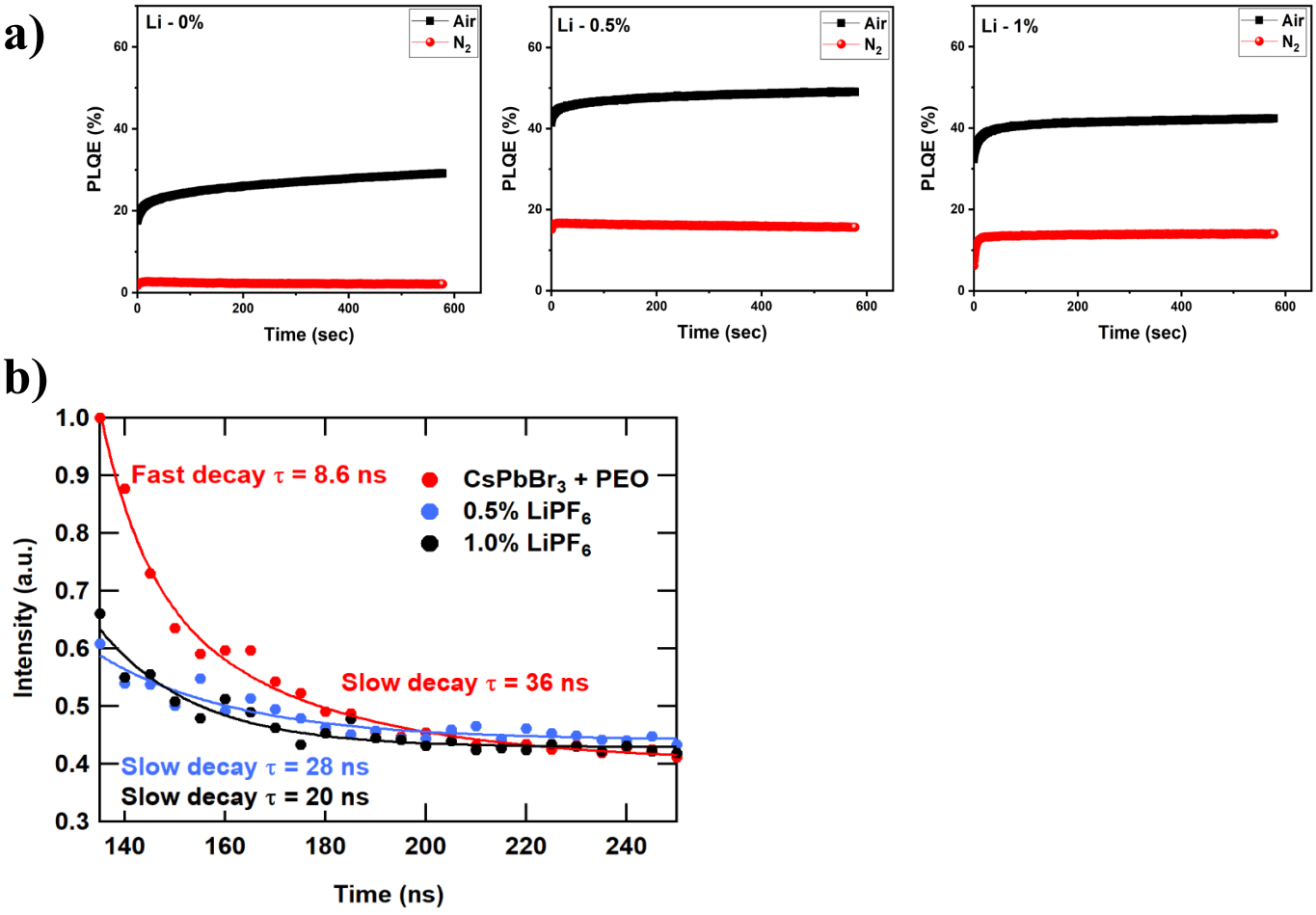

Figure S6. a) Photoluminescence quantum efficiency (PLQE) with time for $CsPbBr_3$:PEO films with 0%, 0.5% and 1.0% LiPF under air or nitrogen environments. Note that in all cases the PLQE is higher in air than nitrogen. Furthermore, the relative change between air (trap suppressing) and nitrogen (trap permitting) is lowered with $LiPF_6$ addition, correlating with lower trap concentration. b) Time-resolved Photoluminescence of $CsPbBr_3$:PEO and $CsPbBr_3$:PEO:$LiPF_6$ thin films.

Supporting Information Table S2

Table S2. Average grain size as measured from SEM and XRD spectral data for $CsPbBr_3$, $CsPbBr_3$:PEO, and $CsPbBr_3$:PEO:$LiPF_6$ thin films.

Sample	Average grain size (nm)	FWHM (degree)	2θ (degree)	Crystallite size (nm)
$CsPbBr_3$	145	0.51	21.53	16.49
		0.50	30.52	17.04
$CsPbBr_3$:PEO (0%)	79	0.52	21.5	16.39
		0.53	30.55	16.15
$CsPbBr_3$:PEO:$LiPF_6$ (0.2%)	105	0.51	21.49	16.47
		0.54	30.59	16.07
CsPbBr3:PEO:$LiPF_6$ (0.5%)	163	0.53	21.49	16.04
		0.57	30.57	15.15
$CsPbBr_3$:PEO:$LiPF_6$ (1%)	166	0.58	21.52	14.56
		0.58	30.58	14.79
$CsPbBr_3$:PEO:$LiPF_6$ (2%)	150	0.61	21.55	13.91
		0.63	30.65	13.71
$CsPbBr_3$:PEO:$LiPF_6$ (5%)	161	0.65	21.6	13.04
		0.65	30.7	13.20

Supporting Information Figure S7

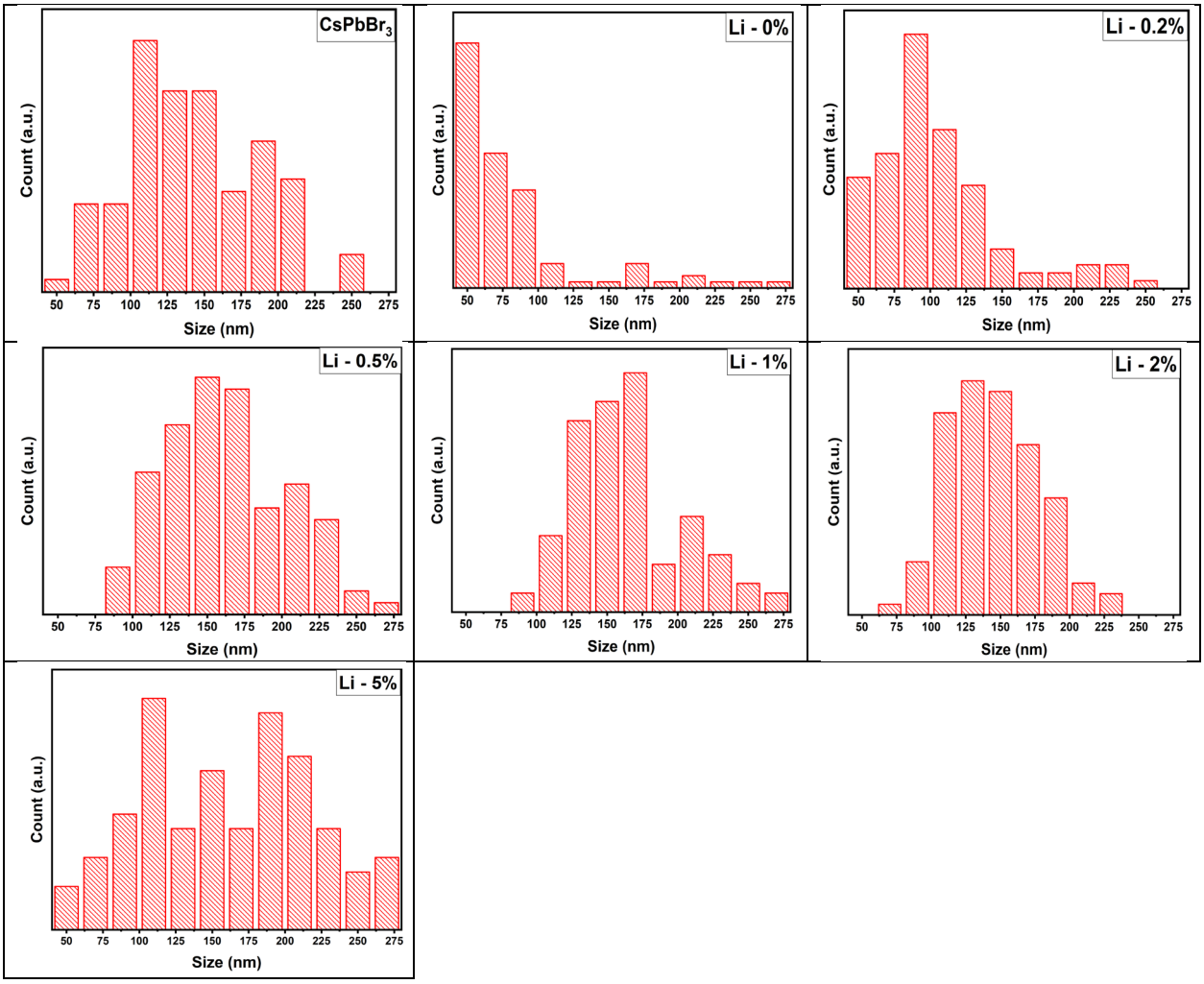

Figure S7. Histograms of $CsPbBr_3$, $CsPbBr_3$:PEO, and $CsPbBr_3$:PEO:$LiPF_6$ thin film grain size as measured from SEM imaging.

Supporting Information Figure S8

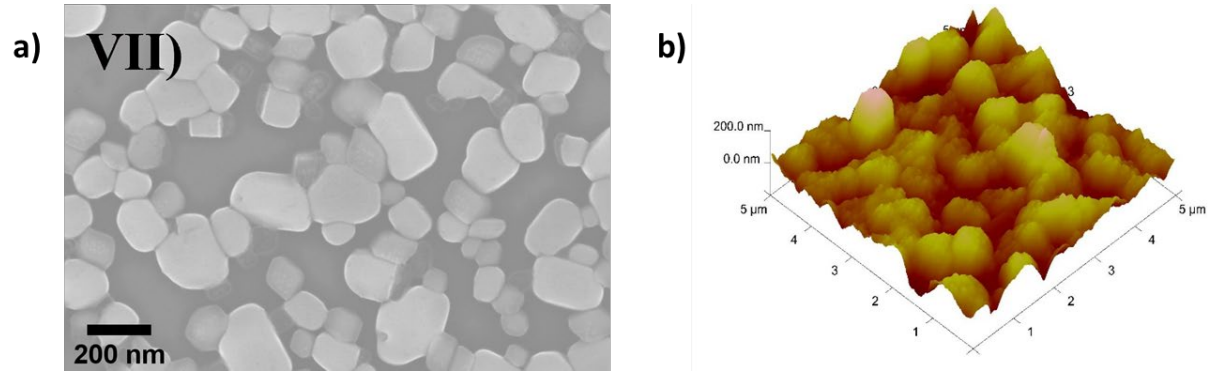

Figure S8. Morphological impact of high $LiPF_6$ concentrations in $CsPbBr_3$:PEO:$LiPF_6$ thin films. a) SEM and b) AFM images of $CsPbBr_3$:PEO:$LiPF_6$ (5%).

Supporting Information Figure S9

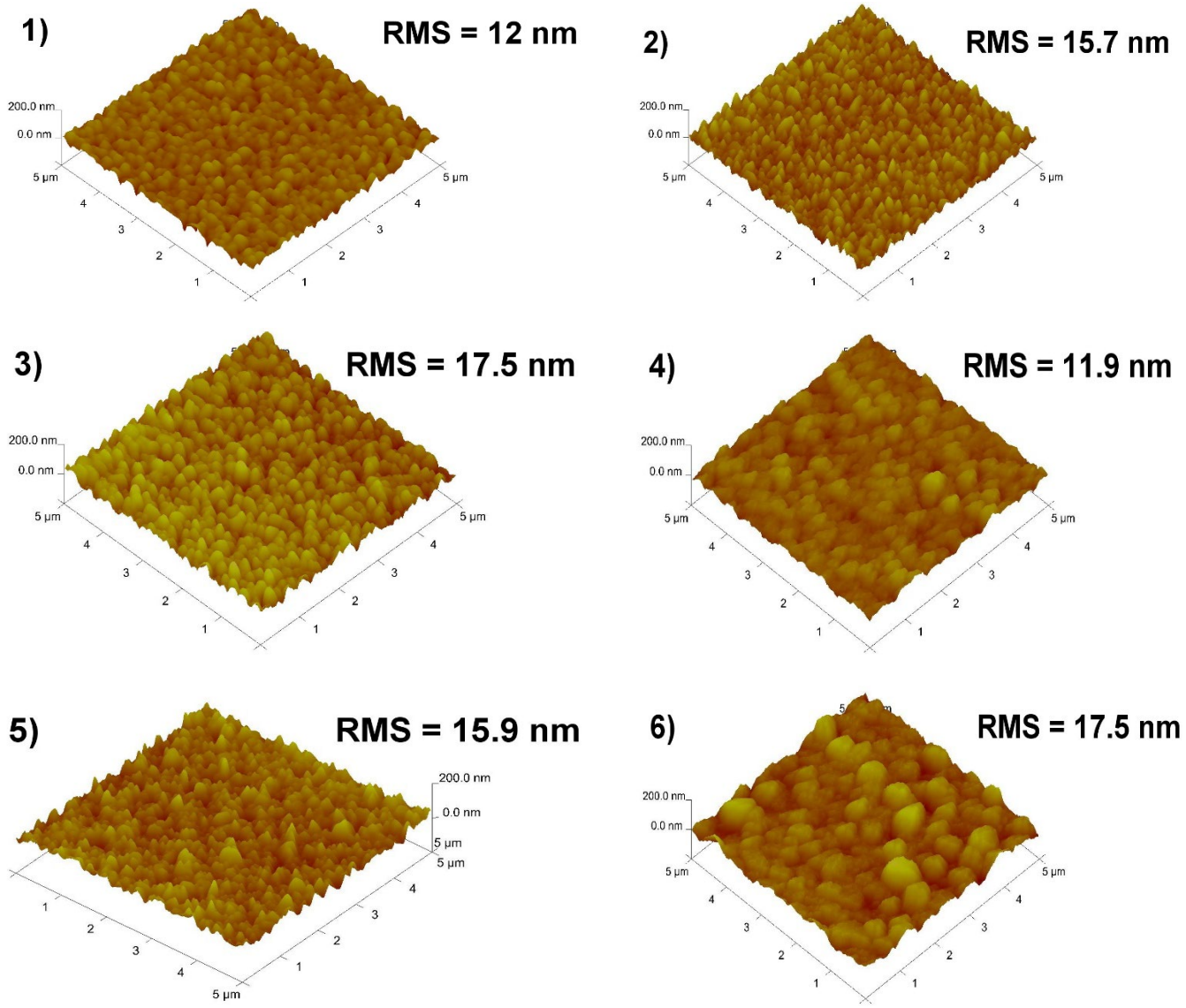

Figure S9. 3D AFM topography images of 1) $CsPbBr_3$, 2) $CsPbBr_3$:PEO (0%), 3) $CsPbBr_3$:PEO:$LiPF_6$ (0.2%), 4) $CsPbBr_3$:PEO:$LiPF_6$ (0.5%), 5) $CsPbBr_3$:PEO:$LiPF_6$ (1%), 6) $CsPbBr_3$:PEO:$LiPF_6$ (2%).

Supporting Information Figure S10

Figure 10. X-Ray photoelectron spectroscopy (XPS) spectra for a) $CsPbBr_3$, b) $CsPbBr_3$:PEO, c) $CsPbBr_3$:PEO:$LiPF_6$ with 0.5 wt% $LiPF_6$ and d) $CsPbBr_3$:PEO:$LiPF_6$ with 2.0 wt% $LiPF_6$.

a) $CsPbBr_3$

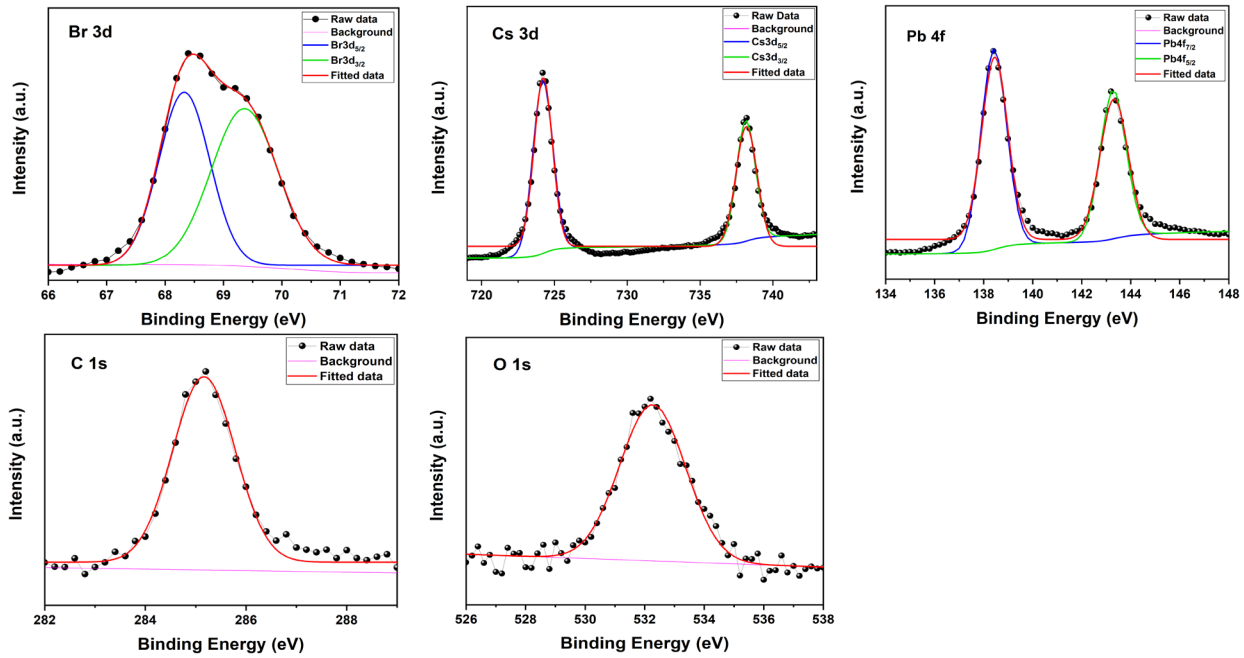

b) $CsPbBr_3$:PEO

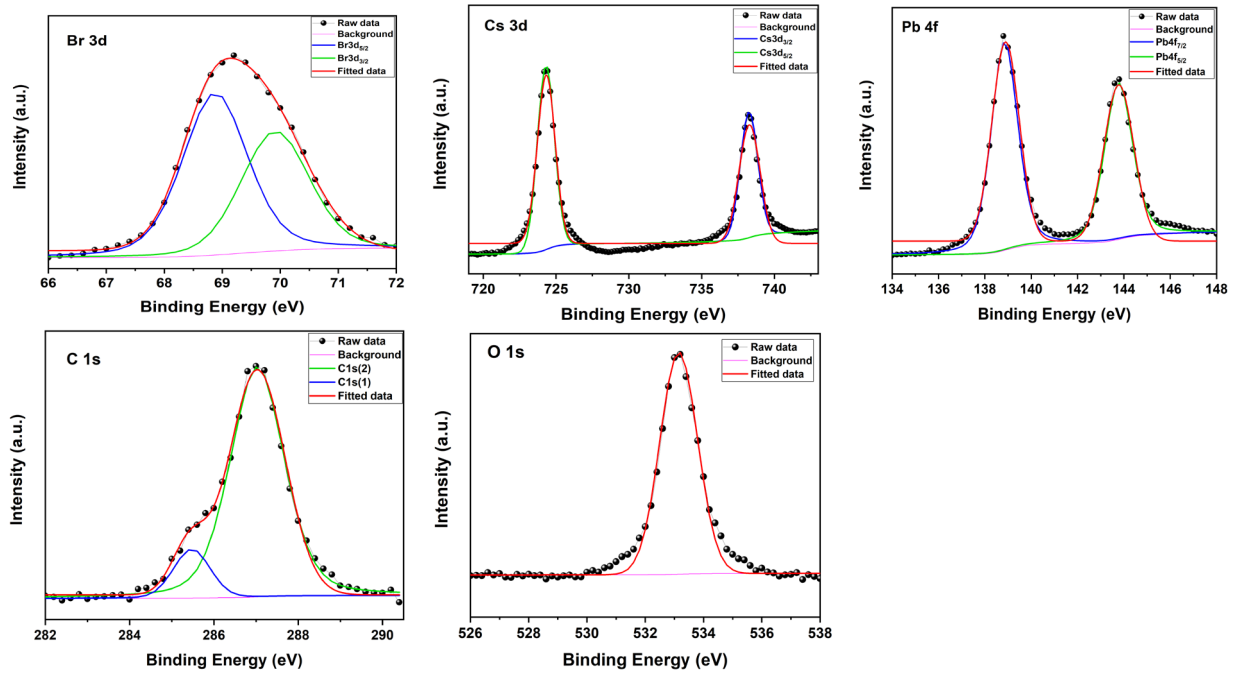

c) $CsPbBr_3$:PEO:$LiPF_6$ (0.5%)

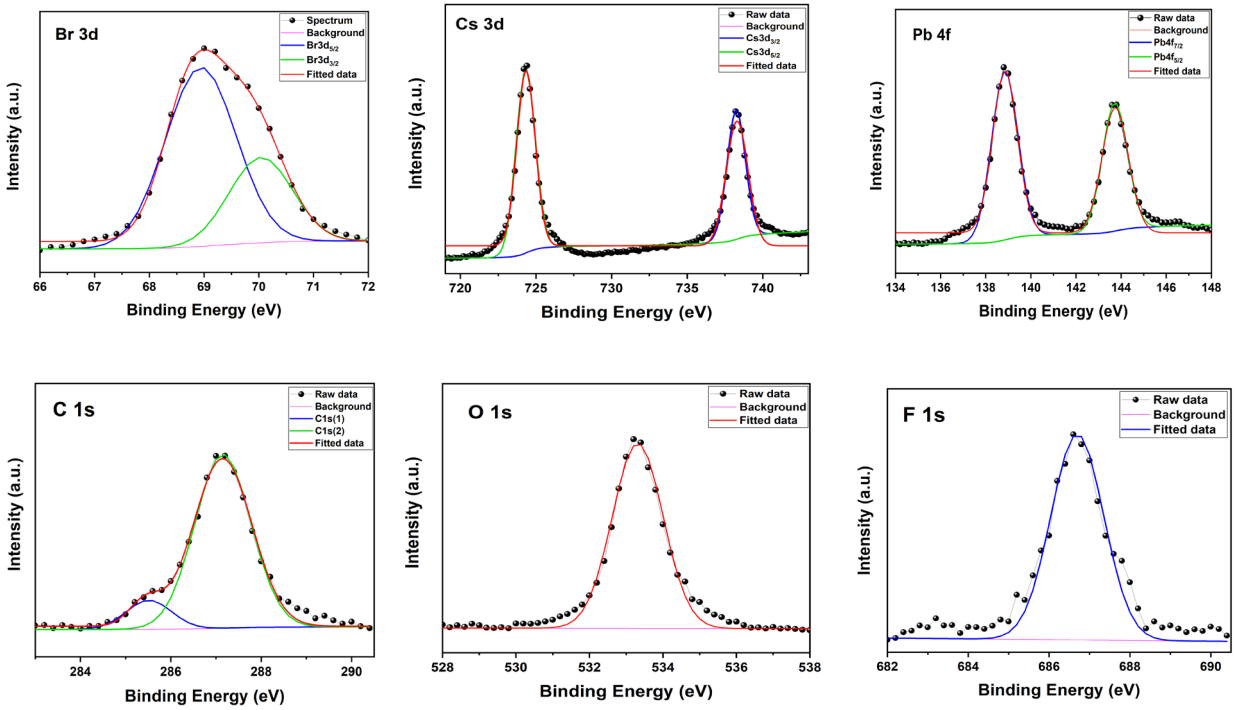

d) $CsPbBr_3$:PEO:$LiPF_6$ (2%)

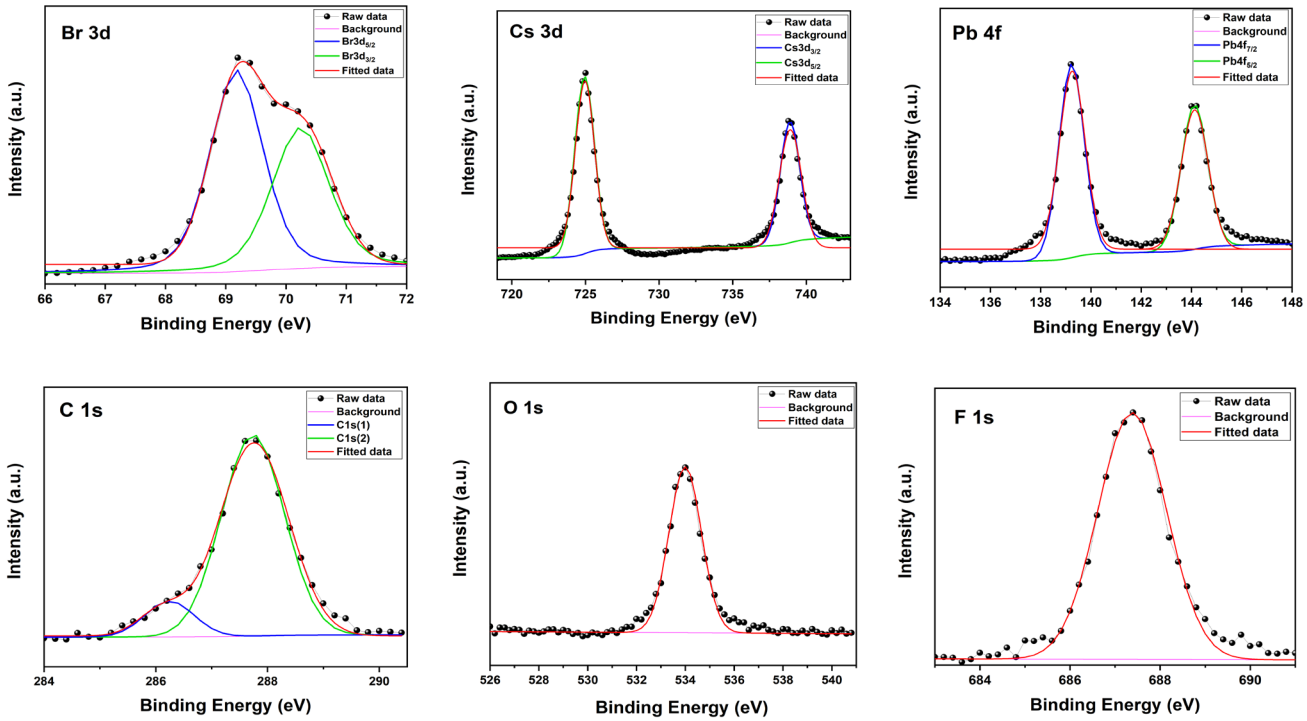

Supporting Information Table S3

Table S3. Comparative performances of the best-in-class perovskite based LEDs and LECs.

Device structure	Single or multilayer	Light Emitting Mechanism	Turn on voltage	Luminescence Max (cd/m2)	Current Efficiency (cd/A)	Power Efficiency (lm/w)	Ref
ITO / PEDOT:PSS /PKNP:TMPE:LiCF3SO3/Al	M	LEC	11	1.8	0.013	-	[2]
ITO / Pero-PEO-composite / In (Ga,Au)	S	LED	3	4064	0.74	-	[3]
ITO / Pero-PEO-PVP-composite / InGa	S	LED	1.9	593178	21.5	14.1	[4]
ITO / PEDOT:PSS /Perovskite / MoO3/Au	M	LEC	2.4	157 (0.23 W/ Sr. m^2)	-	-	[5]
ITO / Pero-PEO composite / Ag NW	S	LED	2.6	21014	4.9	-	[6]
ITO / PEDOT:PSS /MAPbBr3 / SPB-02T /LiF/ Ag	M	LED	2	3490	0.43	0.31	[7]
ITO/PEDOT:PSS/CsPbBr3:PEO/TPBI/ LiF/Al	M	LED	2.6	51890	21.38	14.89	[8]
ITO/PEDOT:PSS/CsPbBr3:PEG/TPBI/ LiF/Al	M	LED	2.5	36600	19	-	[9]
ITO / PEDOT:PSS / $CsPbBr_{1.25}I_{1.75}$ NC: KCF3SO3/Al	M	LEC	4	8	-	-	[10]
VACNT / SC-MAPbBr3 / VACNT	S	LEC	26	1000	-	-	[11]
Our Work	S	LEC	1.9	14730	2.8	3	

Supplement Chapter on Li^+ and other ionic processes in perovskite LEC.

It is important to clarify the location and role of the internal ions in the $CsPbBr_3$:PEO composite and $LiPF_6$ additive of LEC in the formation of electrical double layers (EDLs) at electrodes and doped p-i-n structures given current literature understanding in the field of light emitting electrochemical cells (LECs) and the results of this work. To summarize this understand, we present a detailed schematic of LEC operation in Supporting Figure S11, which shows a cross section of LEC device with perovskite grains separated by the PEO polyelectrolyte matrix (in agreement with our SEM image).

It is likely that $LiPF_6$ is not equally distributed between the perovskite and PEO: at large concentrations of salt (molar ratios 1% to 5%) a majority of it is in the PEO matrix, since Li^+ is known to form a coordination bond with the oxygen atoms of the PEO chains. Subsequently Li^+ moves along the chains facilitated by polymer chain motion (by a hopping process, described by Vogel-Tamman-Fulcher (VTF) equation). So the anticipated Li^+ preference for PEO is based on this interaction and mechanism for high mobility (as illustrated in Figure S11 below). The dissociation and movement of Li^+ by PEO also makes the PF_6^- counterion highly mobile. This leads to a considerable concentration of Li^+ and PF_6^- and at the interface of the perovskite and PEO. Within the perovskite, the internal ions of Br^- and Cs^+ and their vacancies V^+ and V^- all have low activation energies that make them mobile even at room temperature. The small size of Li^+ and PF_6^- ions facilitates diffusion into the perovskite, filling voids and intercalation processes that reduce crystallite size and increase grain size. The details of internal ionic migration have been well studied by electrochemical impedance spectroscopy (EIS) [12] and dynamic capacitance measurements [13]. We present the results of these studies in Table S4, and further discussion will concentrate on the additional effects of the Li^+ and PF_6^- ions on electrical double layer formation, p-i-n structures, and their effect on LEC operation.

(Continued on page S24)

Supporting Information Figure S11

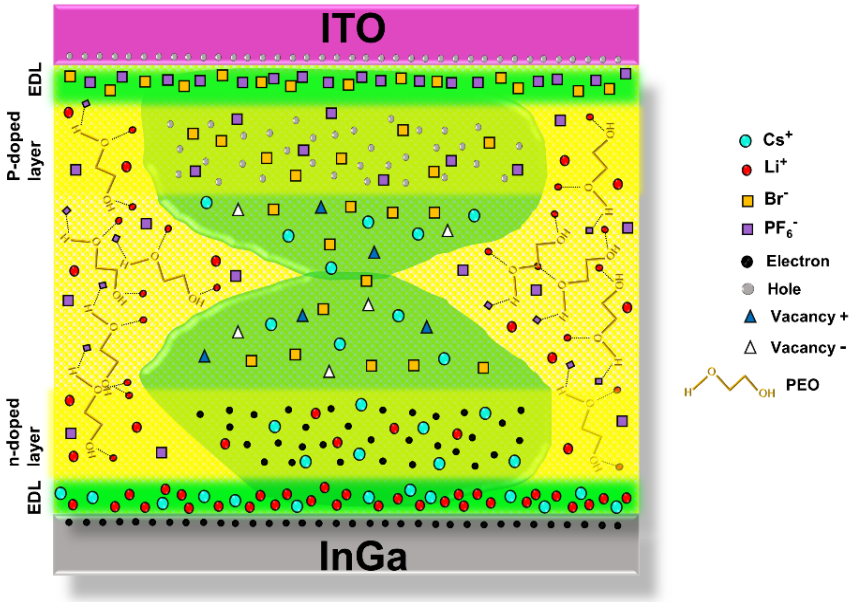

Figure S11. Illustration of the redistribution of ions in $CsPbBr_3$:PEO:$LiPF_6$ thin films.

Supporting Information Figure S12

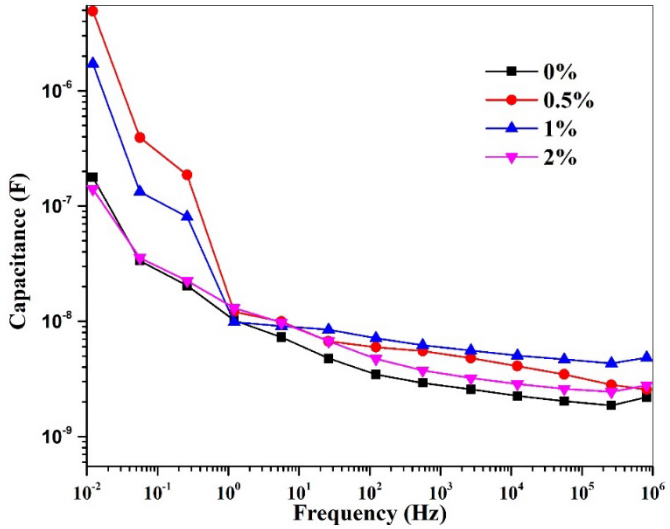

Figure S12. Capacitance versus frequency for Al/$CsPbBr_3$:PEO:$LiPF_6$/PEDOT-PSS/ITO PeLECs with different weight ratios of $LiPF_6$.

Supporting Information Table S4

Table S4. Summrized ionic parameters relevant to PeLECs from literature.

<table>
<tr><th>Ion type and ionic process</th><th colspan="2">Activation Energy (eV)</th><th>Diffusion coefficient ($cm^2 s^{-1}$)</th><th>Mobile ions concentration (cm^{-3})</th><th>Characteristic Times</th><th>Ref</th></tr>
<tr><td rowspan="2">MA^+, FA^+</td><td>Theory</td><td>Experimental</td><td rowspan="2">$(3.4\pm3.3)\ 10^{-12}$</td><td rowspan="2">$(1.3\pm0.8)\ 10^{16}$</td><td rowspan="2">τ=12±0.4 min (EDL by drift of MA^+)</td><td rowspan="2">[13]</td></tr>
<tr><td>0.46-1.12</td><td rowspan="2">Depends on device fabrication</td></tr>
<tr><td>Cs^+ (EDL by cations)</td><td>0.8-2.31</td><td rowspan="2">$(3.1\pm2.8)\ 10^{-9}$</td><td rowspan="2">$(1.1\pm0.9)\ 10^{15}$</td></tr>
<tr><td>I^-, Br^- (EDL by halides)</td><td>0.08-0.58</td><td>0.29±0.06</td><td>τ=30±1.5 s (EDL by halide drift)</td><td>[12]</td></tr>
<tr><td>Li^+</td><td colspan="2">0.24</td><td>10^{-7}</td><td>Varies</td><td>-</td><td>[14,15]</td></tr>
<tr><td>PF_6^-</td><td colspan="2">0.366</td><td>1.18×10^{-13}</td><td>Varies</td><td>-</td><td>[16]</td></tr>
<tr><td>P-doped layer formation</td><td colspan="2"></td><td></td><td></td><td rowspan="2">τ=1.6±0.1 h (growth of charge carriers doped layer via ions)</td><td rowspan="2">[17]</td></tr>
<tr><td>n-doped layer formation</td><td colspan="2"></td><td></td><td></td></tr>
</table>

The formation of EDLs at both electrodes is shown schematically in Figure S11 both in the perovskite and PEO sections, and Li^+ and PF_6^- ions as the smallest and fastest play important roles in several processes:

-at faster and higher charge density EDL formation at the cathode, while small PF_6^- adds to the EDL at anode. In support of this, we observe lower turn on voltages, and here we present a preliminary EIC result of increased capacitance when an optimal $LiPF_6$ concentration is added (Figure S12). Prior studies with LECs from iridium complexes also show this behavior. [20]

- at formation of an n-doped region, similar to n-doping proved by electrochemical doping from outer electrolyte [19] and similarly observed in perovskites with alkali additives [17].

According to transient capacitance measurements and nuclear magnetic resonance studies [13] the perovskite anions (I^-, Br^-) have the greatest diffusion coefficients. Alternatively, the MA^+ or FA^+ cations remain largely stationary, while Cs^+ is considerably more mobile. Basic parameters for mobile ions in perovskites are summarized in Table S4, which also shows characteristic times of dynamical processes of EDL formation and p- doped and n-doped layers formation times, which are changed by Li-salt additions. We have chosen $LiPF_6$ salt, since the PF_6^- counterion has shown the fastest dynamics among other counter-ions in traditional LEC (e.g. $LiBF_4$, being slowest), due to facile dissociation into Li^+ and PF_6^-.[19] Small Li^+ ion also exhibits fast diffusion when intercalated into a perovskite matrix, as shown by electrochemical doping by Li from outer electrolytes [8] and Li^+ migration across a perovskite layer from Spiro-OMeTAD to TiO_2 in solar cells [17].

The dynamics of ionic migration studied by Puscher *et al.* [12] are clearly revealed in our devices, as shown in Figure S13. In particular, the tri-exponential behaviour of current vs time in LEC reveals following changes by adding Li^+:

1) The fastest time ($t < 0.2$ h) corresponds to formation of EDL at anode, by accumulation of halide: in our case Br^- ions, and PF_6^- when salt is added.
2) The second time ($0.2\ h < t < 2\ h$) is the EDL formation by cations: either slowest MA^+ in MAPI or Cs^+ in our case for 0% devices. When Li^+ is added, the formation of EDL at cathode becomes faster and greater charge is accumulated, as seen for the 0.5% $LiPF_6$ device. This is also confirmed by the higher capacitance at low frequencies shown in Figure S12. (More details will be revealed in a forthcoming paper).
3) The slowest process ($t > 2h$) is the formation of the p-i-n structure by slow accumulation of ions/carrier diffusion propagating from the EDLs to the bulk. (See Table S4 for characteristic times.)

So summarizing the preliminary observations of Li^+ effects, we conclude that optimal Li^+ concentration improves both EDLs and n-doping (making its formation also faster, due to faster diffusion via the small size of Li^+).

Supporting Information Figure S13

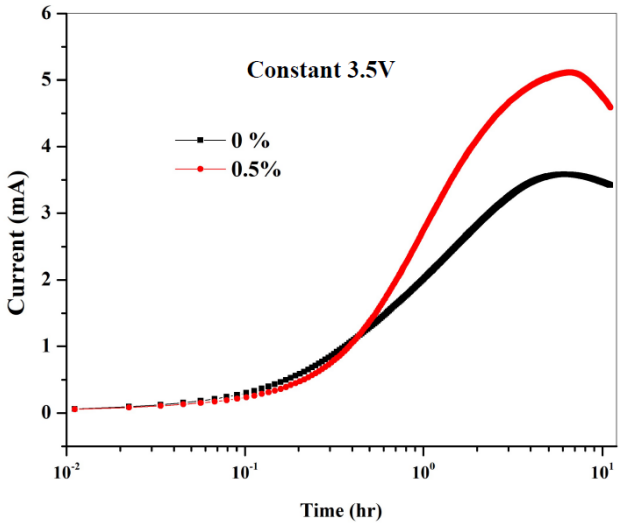

Figure S13. Current versus time (logarithmic scale) for 3.5 V constant voltage operation of Al/$CsPbBr_3$:PEO:$LiPF_6$/PEDOT-PSS/ITO LEC devices with different weight ratios of $LiPF_6$.

References

[1] J. C. De Mello, H. F. Wittmann and R. H. Friend, "An improved experimental determination of external photoluminescence quantum efficiency," *Advanced Materials,* vol. 9, no. 3, pp. 230-232, 1997.

[2] M. F. Ayguler, M. D. Weber, B. M. D. Puscher, D. D. Medina, P. Docampo and R. D. Costa,,, "Light-Emitting Electrochemical Cells Based on Hybrid Lead Halide Perovskite Nanoparticles," *J. Phys. Chem. C,* vol. 119, p. 12047–12054, 2015.

[3] Junqiang Li, Sri Ganesh R. Bade, Xin Shan and Zhibin Yu, "Single-Layer Light-Emitting Diodes Using Organometal Halide Perovskite/Poly(ethylene oxide) Composite Thin Films," *Adv.Mater.,* vol. 27, p. 5196–5202, 2015.

[4] Junqiang Li, Xin Shan, Sri Ganesh R. Bade, Thomas Geske, Qinglong Jiang, Xin Yang and Zhibin Yu, "Single-Layer Halide Perovskite Light-Emitting Diodes with Sub-Band Gap Turn-On Voltage and High Brightness," *The Journal of Physical Chemistry Letters ,* vol. 7, no. 20, pp. 4059-4066, 2016.

[5] Huimin Zhang , Hong Lin , Chunjun Liang , Hong Liu , Jingjing Liang , Yong Zhao , Wenguan Zhang , Mengjie Sun , Weikang Xiao , Han Li , Stefano Polizzi , Dan Li ,Fujun Zhang , Zhiqun He , and Wallace C. H. Choy , "Organic–Inorganic Perovskite Light-Emitting Electrochemical Cells with a Large Capacitance," *Adv. Funct. Mater. ,* vol. 25, p. 7226–7232, 2015.

[6] Sri Ganesh R. Bade, Junqiang Li, Xin Shan, Yichuan Ling, Yu Tian, Tristan Dilbeck, Tiglet Besara, Thomas Geske, Hanwei Gao, Biwu Ma, Kenneth Hanson, Theo Siegrist, Chengying Xu and Zhibin Yu, "Fully Printed Halide Perovskite Light-Emitting Diodes with Silver Nanowire Electrodes," *ACS Nano,* vol. 10, no. 2, pp. 1795-1801, 2016.

[7] Jae Choul Yu, Da Bin Kim, Eui Dae Jung, Bo Ram Lee and Myoung Hoon Song, "High-performance perovskite light-emitting diodes via morphological control of perovskite films," *Nanoscale,* vol. 8, pp. 7036-7042 , 2016.

[8] Chen Wu, Yatao Zou, Tian Wu, Muyang Ban, Vincenzo Pecunia, Yujie Han, Qipeng Liu, Tao Song, Steffen Duhm and Baoquan Sun, "Improved Performance and Stability of All-Inorganic Perovskite Light-Emitting Diodes by Antisolvent Vapor Treatment," *Adv. Funct. Mater.,* vol. 27, p. 1700338, 2017.

[9] Li Song, Xiaoyang Guo, Yongsheng Hu, Ying Lv, Jie Lin, Zheqin Liu, Yi Fan and Xingyuan Liu, "Efficient Inorganic Perovskite Light-Emitting Diodes with Polyethylene Glycol Passivated Ultrathin CsPbBr3 Films," *The Journal of Physical Chemistry Letters,* vol. 8 , no. 17, pp. 4148-4154, 2017.

[10] Meltem F Aygüler, Bianka M D Puscher, Yu Tong, Thomas Bein, Alexander S Urban, Rubén D Costa and Pablo Docampo, "Light-emitting electrochemical cells based on inorganic metal halide perovskite nanocrystals," *J. Phys. D: Appl. Phys,* vol. 51, pp. 334001-334007, 2018.

[11] Pavao Andričević, Xavier Mettan, Márton Kollár, Bálint Náfrádi, Andrzej Sienkiewicz, Tonko Garma, Lidia Rossi, László Forró, and Endre Horváth, "Light-Emitting Electrochemical Cells of Single Crystal Hybrid Halide Perovskite with Vertically Aligned Carbon Nanotubes Contacts," *ACS Photonics,* vol. 6 , no. 4, pp. 967-975, 2019.

[12] Bianka M. D. Puscher, Meltem F. Aygüler, Pablo Docampo, Rubén D. Costa, "Unveiling the Dynamic Processes in Hybrid Lead Bromide Perovskite Nanoparticle Thin Film Devices," *Adv. Energy Mater.,* vol. 7, pp. 1602283-1602292, 2017.

[13] Moritz H. Futscher, Ju Min Lee, Lucie McGovern, Loreta A. Muscarella, Tianyi Wang, Muhammad Irfan Haider, Azhar Fakharuddin, Lukas Schmidt-Mende and Bruno Ehrler, "Quantification of ion migration in CH3NH3PbI3 perovskite solar cells by transient capacitance measurements," *Mater. Horiz., ,* vol. 6, pp. 1497-1503, 2019.

[14] Nuria Vicente and Germà Garcia-Belmonte, "Organohalide Perovskites are Fast Ionic Conductors," *Adv. Energy Mater.,* vol. 7, pp. 1700710-1700714, 2017.

[15] Yifei Suna, Michele Kotiugab, Dawgen Lim, "Strongly correlated perovskite lithium ion shuttles and Shriram Ramanathana," *Proceedings of the National Academy of Sciences,* vol. 115, no. (39) , pp. 9672-9677, 2018.

[16] Seiji Miyoshi, Taner Akbay, Takuya Kurihara, Taro Fukuda, Aleksandar Tsekov Staykov, "Fast Diffusivity of PF6– Anions in Graphitic Carbon for a Dual-Carbon Rechargeable Battery with Superior Rate Property," *J. Phys. Chem. C ,* vol. 120, p. 22887−22894, 2016.

[17] Clara Aranda, Antonio Guerrero, and Juan Bisquert, "Ionic Effect Enhances Light Emission and the Photovoltage of Methylammonium Lead Bromide Perovskite Solar Cells by Reduced Surface Recombination," *ACS Energy Lett. ,* vol. 4, p. 741−746, 2019.

[18] E. Bandiello, M. Sessolo and H. J. Bolink, "Lithium salt additives and the influence of their counterion on the performances of light-emitting electrochemical cells," *J. Mater. Chem. C,* vol. 4, pp. 10781-10785, 2016.

[19] Qinglong Jiang, Mingming Chen, Junqiang Li, Mingchao Wang, Xiaoqiao Zeng, Tiglet Besara, Jun Lu, Yan Xin, Xin Shan, Bicai Pan, Changchun Wang, Shangchao Lin, Theo Siegrist, Qiangfeng Xiao, and Zhibin Yu , "Electrochemical Doping of Halide Perovskites with Ion Intercalation," *ACS Nano,* vol. 11, p. 1073−1079, 2017.

[20] Lyndon D. Bastatas, Kuo-Yao Lin, Mattew D. Moore, Kristin J. Suhr, Melanie H. Bowler, Yulong Shen, Bradley J. Holliday and Jason D. Slinker. Discerning the Impact of a Lithium Salt Additive in Thin-Film Light-Emitting Electrochemical Cells with Electrochemical Impedance Spectroscopy. *Langmuir* vol. 32, p. 9468-9474, 2016.